

TO

SIVARAM AND PARENTS

THE DIFFUSION OF  $\text{Co}^{60}$  IN  $\text{Zr}_{50}\text{Ti}_{50}$  ALLOY

S. Kumar B.Sc., M.Sc.

Department of Physics

(Submitted in partial fulfillment of  
the requirements for the degree of

Master of Science)

B R O C K U N I V E R S I T Y

St. Catharines, Ontario

September 1973

167128

# ABSTRACT

The diffusion of  $\text{Co}^{60}$  in the body centered cubic beta phase of a  $\text{Zr}_{50}\text{Ti}_{50}$  alloy has been studied at  $900^\circ$ ,  $1200^\circ$ , and  $1440^\circ\text{C}$ . The results confirm earlier unpublished data obtained by Kidson<sup>17</sup>. The temperature dependence of the diffusion coefficient is unusual and suggests that at least two and possibly three mechanisms may be operative.

Annealing of the specimen in the high B.C.C. region prior to the deposition of the tracer results in a large reduction in the diffusion coefficient. The possible significance of this effect is discussed in terms of rapid transport along dislocation network.

### Acknowledgements

The author wishes to acknowledge the many helpful discussions and encouragement given by his thesis supervisor, Dr. G. V. Kidson.

It is a pleasure to thank the technical staff of Brock University, Mr. Harry Laird and Mr. George Zibens for their assistance during the course of the present study.

The assistance given by Mr. Jerry Dobruk and Mr. Skipper Poehlman in numerical calculations is greatly appreciated.

Special thanks are due to Mrs. Joyce Cowan, for having typed this manuscript with great speed and accuracy.

Financial support for this project has come from the National Research Council of Canada, which is greatly appreciated.



# TABLE OF CONTENTS

CHAPTER I	INTRODUCTION	1
CHAPTER II	THEORY	12
	II.1. Fick's Laws	12
	II.2. Macroscopic Considerations	14
	II.3. Random Walk	15
	II.4. Temperature dependence of the diffusion coefficient	17
CHAPTER III	EXPERIMENTAL TECHNIQUE	21
	III.1. Temperature Controller (Recorder Assembly)	22
	III.2. Calibration of the thermocouple	22
	III.3. Preparation of the specimens	23
	III.4. Evaporation of tracer	25
	III.5. Diffusion anneal	25
	III.6. Sectioning Method	27
	III.7. Measurement of specific activity	28
	III.8. Diffusion coefficient	28
CHAPTER IV	RESULTS	40
	IV.1. Calibration of the thermocouple	40
	IV.2. Diffusion Measurements	41
	IV.3. Preannealing experiments	41
CHAPTER V	DISCUSSION	59
	CONCLUSIONS	65
APPENDIX A.	Solution to Fick's equation	73
APPENDIX B.	Measurement of tracer concentration	75
APPENDIX C.	General treatment of random walk processes	80
APPENDIX D.	Concerning the "tail" in the penetration profiles	88
	REFERENCES	90

# LIST OF ILLUSTRATIONS

<u>FIGURES</u>	<u>Page No.</u>
Fig. 1.1 Self diffusion in beta zirconium	4
Fig. 1.2 Self and Solute diffusion in beta zirconium.	5
Fig. 1.3 Diffusion of $\text{Co}^{60}$ in beta zirconium.	8
Fig. 1.4 Melting point and phase diagram for Zr-Ti alloy.	9
Fig. 1.5 Arrhenius plot for diffusion of $\text{Co}^{60}$ in $\text{Zr}_{50}\text{Ti}_{50}$ .	10
Fig. 3.1 The heating circuit.	26
Fig. 4.1 Determination of the melting point of gold.	45
Fig. 4.2 Determination of the melting point of platinum.	46
Fig. 4.3 Diffusion of $\text{Co}^{60}$ in $\text{Zr}_{50}\text{Ti}_{50}$ at $900^{\circ}\text{C}$ for 2 hours.	47
Fig. 4.4 Diffusion of $\text{Co}^{60}$ in $\text{Zr}_{50}\text{Ti}_{50}$ at $900^{\circ}\text{C}$ for 2 hours.	48
Fig. 4.5 " " " $1200^{\circ}\text{C}$ " 82 minutes.	49
Fig. 4.6 " " " " " " "	50
Fig. 4.7 " " " $1440^{\circ}\text{C}$ " 25 minutes.	51
Fig. 4.8 " " " " " " "	52
Fig. 4.9 Penetration profile for preannealed run at $900^{\circ}\text{C}$ .	53
Fig. 4.10 A portion of the above on a large scale.	54
Fig. 4.11 Reproducibility of data for the runs at $900^{\circ}\text{C}$ .	55
Fig. 4.12 " " " " " " at $1200^{\circ}\text{C}$ .	56
Fig. 4.13 " " " " " " at $1440^{\circ}\text{C}$ .	57
Fig. 4.14 Arrhenius plot for diffusion of $\text{Co}^{60}$ in $\text{Zr}_{50}\text{Ti}_{50}$ .	58
Fig. B.1 Schematic diagram for the measurement of the tracer concentration.	76
Fig. B.2 Schematic diagram for the calibration of the single channel analyser.	77
Fig. B.3 Gated $\text{Co}^{60}$ spectrum.	79

<u>PLATES</u>	<u>Page No.</u>
Plate 1     Apparatus for tracer evaporation.	66
Plate 2     Temperature controller/recorder assembly.	67
Plate 3     Top view of the lathe, with the tool in position.	68
Plate 4     Collecting funnel surrounding the specimen.	69
Plate 5     Detection and scaling devices.	70
Plate 6     Diffusion furnace.	71
Plate 7     High temperature evaporation apparatus.	72

## LIST OF TABLES

	<u>Page No.</u>
Table III.1. Chemical analysis of zirconium	24
Table IV.1. Calibration of W-Re thermocouple.	40
Table IV.2. Parameters used in diffusion runs.	42
Table IV.3. Thermal history of specimen prior to tracer deposition.	43
Table V.1 Calculation of dislocation density.	64

## CHAPTER I. INTRODUCTION

It is an experimentally observed fact that the atoms in a crystal can migrate through the lattice. This migration of atoms is termed "diffusion". A macroscopic measure of the rate of migration is given by the "diffusion coefficient"  $D$ , which, in the simplest case, can be defined as the ratio of the flux  $J$  of atoms per unit area per second to the concentration gradient,

$$\text{i.e., } D = - J / \text{Grad } C \quad (1.1)$$

Accurate and reproducible measurements of  $D$  have been made for a large number of systems using a variety of techniques. Of the latter, the most useful have involved radioactive tracer atoms in either single crystals or large grained systems.

Fundamental studies have been primarily concerned with the identification of the mechanism or mechanisms by which the atoms move. In most face centered cubic (f.c.c.) metals, there is strong evidence to indicate that this takes place via a series of place exchanges with near neighbor vacancies (1).

More recently, considerable interest has shifted toward the diffusion behavior of body centered cubic (b.c.c.) metals. This is largely due to a combination of the growing technological importance of the refractory metals, to their increasing purity and to a natural extension of fundamental interest in these systems. As a result, there has been considerable effort to measure diffusion in b.c.c. metals, and the results have shown that the diffusion behavior of at least some might differ fundamentally from that of the other metals.

These are  $\beta$ -Zr ( 2,3 ),  $\beta$ -Ti ( 4 ) and  $\delta$ -U ( 5 ).

On the basis of the experimental evidence available, the b.c.c. metals fall into two fairly distinct groups with regard to their diffusion behavior; these have come to be referred to as

(i) Normal metals and (ii) Anomalous metals.

In the following, the features that characterize "normal" behavior are described; these are then taken as a guideline in identifying the anomalous behavior of the second group.

#### I. 1. NORMAL DIFFUSION

There are three essential features of self diffusion that characterize normal behavior:

(i) The temperature dependence of the diffusion coefficient  $D$ , is described by the Arrhenius relation.

$$D = D_0 \exp (-Q/RT) \quad (1.2)$$

in which  $Q$ , the activation energy and  $D_0$ , the frequency factor, are temperature independent.

(ii)  $Q$  is roughly proportional to the melting point,  $T_m$ .

For self diffusion in metals ( 6 )

$$Q \approx 34 T_m \text{ cal/mole} \quad (1.3)$$

There are other correlations, such as

$$Q \approx 16.5 L_m \text{ cal/mole} \quad (1.4)$$

where  $L_m$  is the latent heat of melting.

While these are empirical relationships, they are followed by a wide range of metals and are useful in providing an approximate value for the activation energy in the absence of experimental data.

(iii) The pre-exponential factor  $D_0$  usually lies within an order of magnitude of 0.5, that is

$$0.05 \leq D_0 \leq 5.0 \text{ cm}^2/\text{sec.}$$

Zener (7) has shown from thermodynamic considerations that this is to be expected for the vacancy mechanism.

## I. 2. ANOMALOUS METALS

According to equation (1.2), a plot of the logarithm of the diffusion coefficient versus the reciprocal of the absolute temperature should be linear. For the anomalous metals  $\beta$ -Zr,  $\beta$ -Ti and  $\gamma$ -U, however, this Arrhenius plot for self diffusion shows a continuous curvature, as exemplified by self diffusion in  $\beta$ -Zr (3) and shown in figure 1.1.

A marked non-linearity has also been observed for impurity diffusion in the b.c.c. phases of Zirconium, Titanium and Uranium (8), as shown in figure 1.2.

These anomalous metals exhibit a further unusual feature in that the coefficients for both self and solute diffusion are remarkably high.

Several proposals have been suggested to account for the curved Arrhenius plot.

If it is assumed that the results are due to a single mechanism of diffusion, the parameters  $D_0$  and  $Q$  must be markedly temperature-dependent (9).

This assumption alone, of course, does not account for the unusually rapid self diffusion, nor the extraordinarily high diffusion rates of impurities and it fails to explain the lack of observable curvature in normal metal systems. Kidson and Kirkaldy (10) have

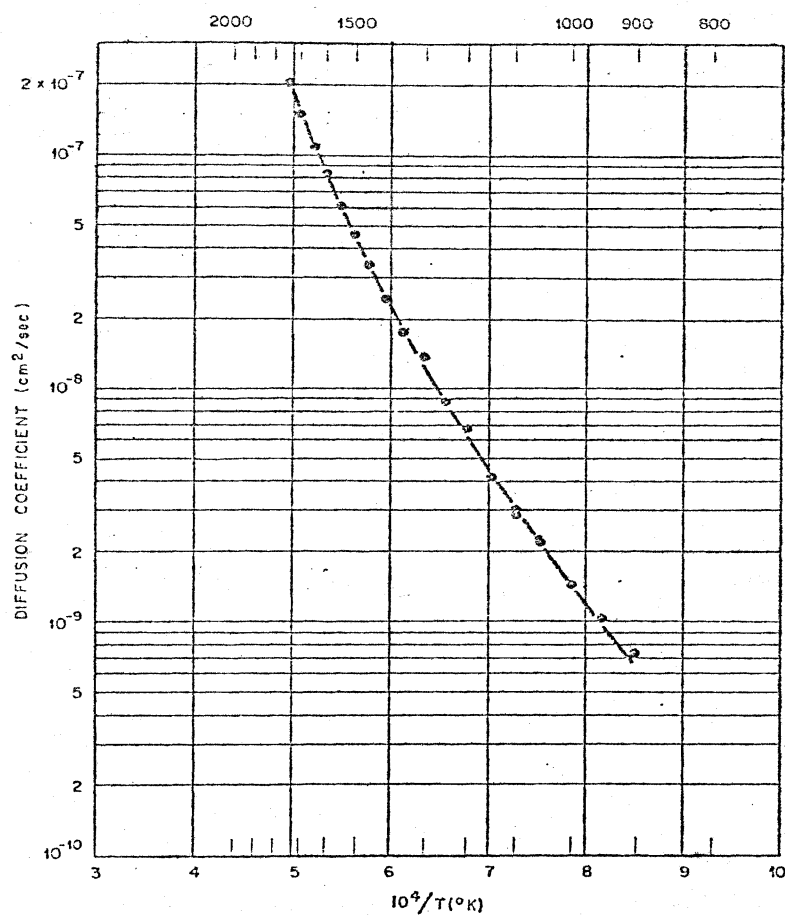


Figure 1.1. Self Diffusion in Zirconium

[ J.I.Federer and T.S.Lundy, Trans AIME 227 592 (1963) ]



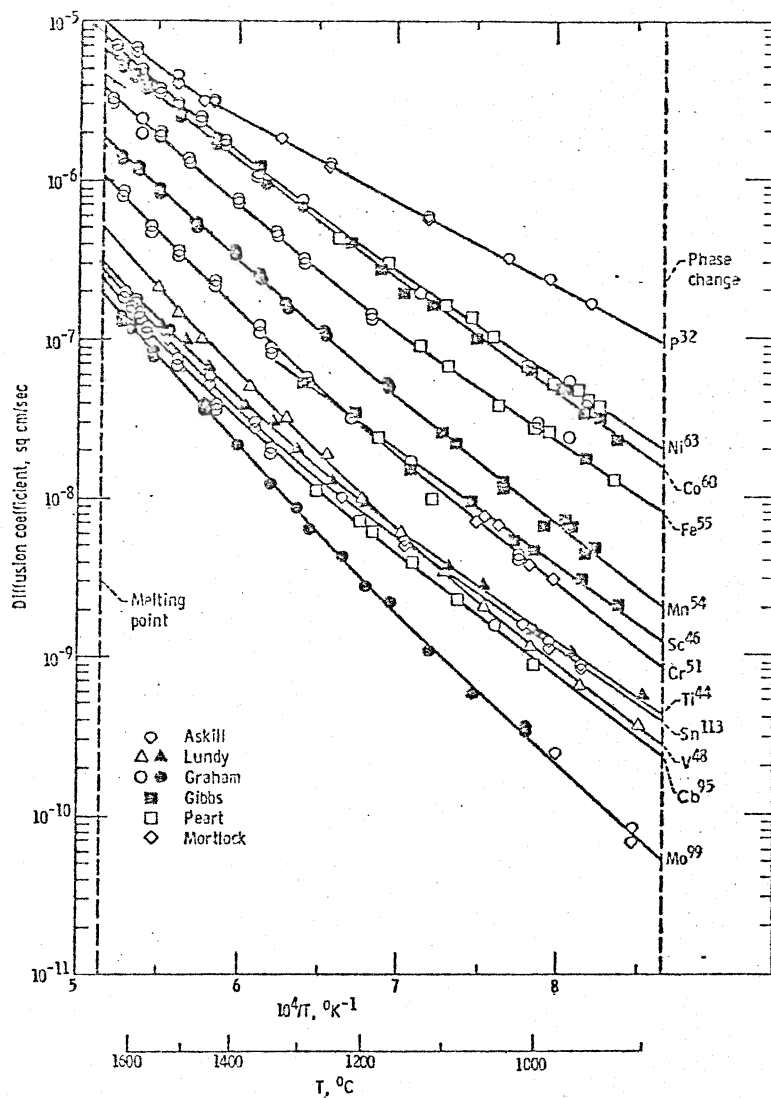


Figure 1.2. Self and Solute Diffusion in Titanium

[ D.Graham, Diffusion in Body Centered Cubic Metals.  
Cleveland, Ohio: American Society for Metals, p 27 ]

shown that the assumption of the vacancy mechanism acting alone is inconsistent with their experimental observations for  $\beta$ -Zr.

An alternative proposal is that two or more mechanisms are operative so that the observed diffusion coefficient is a composite of the contributing mechanisms.

In favorable circumstances; that is, when the parameters associated with the several mechanisms are sufficiently different, a composite Arrhenius curve may be resolved into its components. On the other hand, if the parameters are close, the resolution of a curved Arrhenius plot becomes difficult and in the case of self diffusion in  $\beta$ -Zr, for example, is quite ambiguous (10). Nevertheless, in the latter case, the Arrhenius plot has been represented as the sum of two linear components, and considerable evidence suggests that at the high temperatures the vacancy mechanism is dominant (11).

If such is the case, the problem then reduces to identifying the low-temperature mechanism. Several have been suggested; these include the enhancement of the vacancy concentration by impurities (12), rapid diffusion along dislocations and/or grain boundaries (13), and for solute diffusion, migration along interstitial sites (14).

It was first pointed out by Gruzin et al. (15) that all of the anomalous metals pass from the room temperature close packed hexagonal crystal structure to the high temperature body centered cubic structure via a martensitic phase change. This phase change introduces a large dislocation concentration which could account for the enhanced

diffusion rates at the lower temperatures.

Recently, Kidson and Young (16) found that the Arrhenius plot for the diffusion of  $\text{Co}^{60}$  in  $\beta$  Zr was linear over a wide range of temperatures, as shown in figure 1.3, although there was an indication of some positive curvature above  $1600^\circ\text{C}$ .

More recently, Kidson (17) studied the diffusion of  $\text{Co}^{60}$  in a 50 at % Zr - 50 at % Ti alloy in which the b.c.c. structure is retained down to  $525^\circ\text{C}$ , as shown in figure 1.4. The primary aim of this study was to further explore the significance of a lack of curvature for diffusion of  $\text{Co}^{60}$  in b.c.c. Zr (16). The results of the measurements are shown in figure 1.5.

As can be seen, this plot is linear in the temperature range  $600^\circ - 1100^\circ\text{C}$ , above which a positive curvature occurs. This is followed, however, by a negative curvature, an effect never before reported.

The above considerations lead to the following tentative interpretation; in the low temperature region the diffusion rates are dominated by migration along dislocations; the positive curvature arises as the vacancy mechanism begins to make a significant contribution to the total diffusion.

The subsequent negative curvature could then result if the non-equilibrium dislocation density began to anneal out at the high temperatures, thereby lowering its contribution to the total diffusion.

Alternatively, the unusual high temperature observations could be ascribed to an error in the temperature measurements.

The objects of the present investigation are thus threefold:

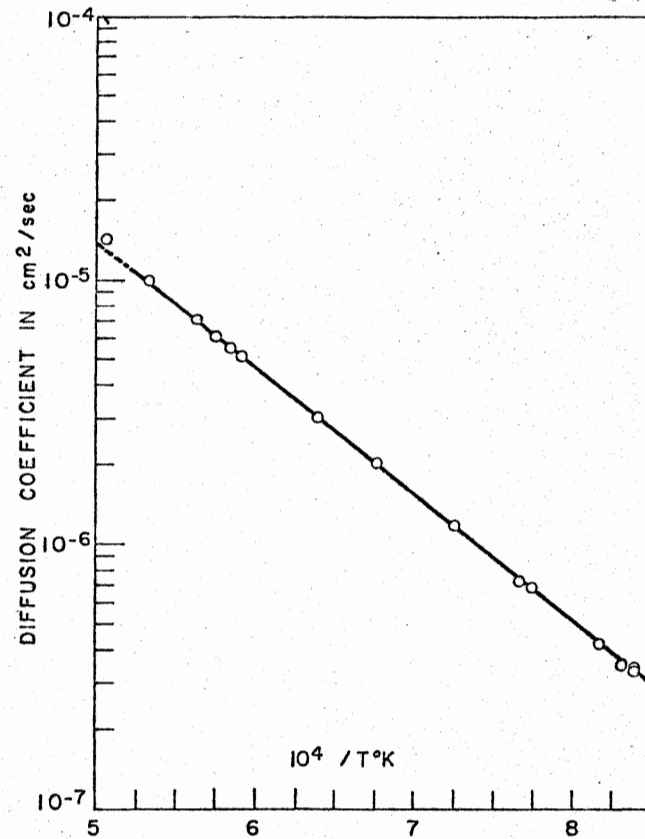


Fig.1.3. The Arrhenius plot for the diffusion of  $^{60}\text{Co}$  in b.c.c. zirconium, showing the absence of curvature between  $875^\circ\text{C}$  and  $1600^\circ\text{C}$ .

[ G.V.Kidson and G.J.Young, Phil Mag 20 1047 (1969) ]

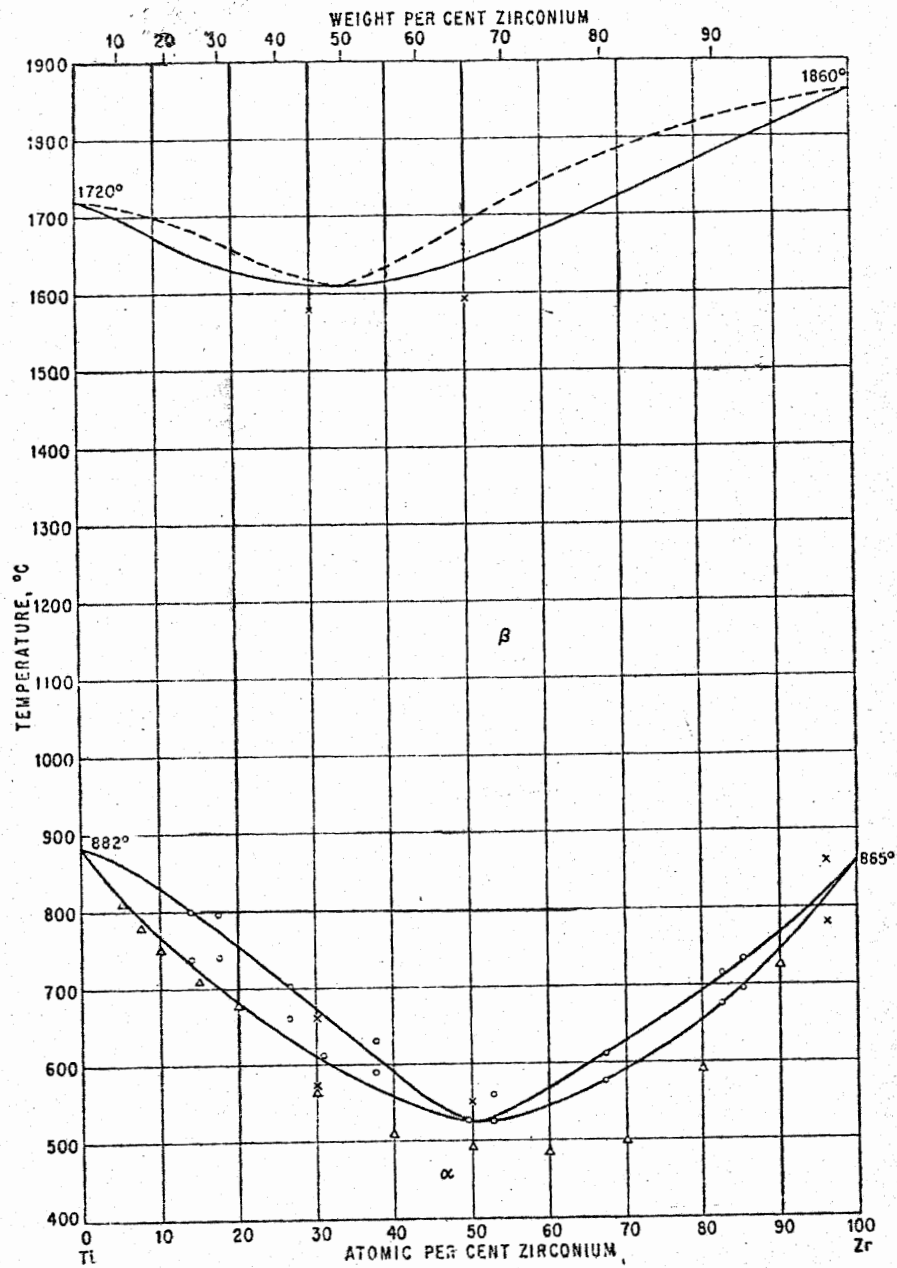
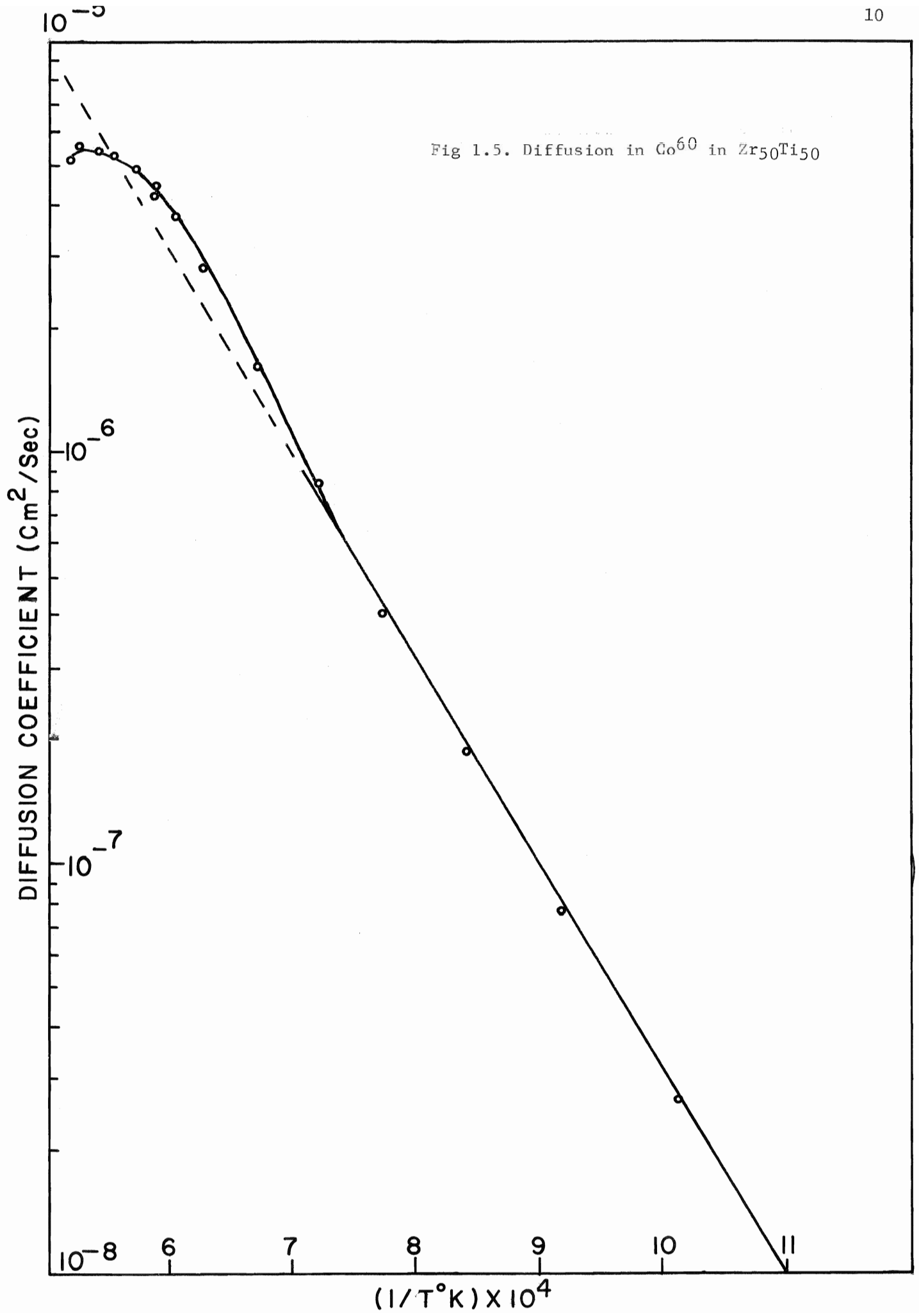


Figure 1.4. Melting Point and Phase Diagram for Zr-Ti Alloy.

[ Hansen, Constitution of Binary Alloys,  
McGraw Hill Book Co., p 1244 (1958)]



(i) to check the reliability of the temperature measurements by recalibrating the thermocouple;

(ii) to establish the reproducibility of the experimental results; and

(iii) to observe the effects of prolonged preannealing of the specimen at a high temperature, prior to deposition of the radioactive tracer. In particular, to construct an apparatus that permits the deposition of the tracer layer while maintaining the specimen in the b.c.c. phase. If the observed diffusion coefficient is reduced, this would then support the dislocation model.

## CHAPTER II. THEORY

The equations governing the diffusion processes are reviewed in section 1. The diffusion coefficient is related to macroscopic parameters in section 2 and to microscopic parameters in section 3. In section 4, the form of the temperature dependence of the diffusion coefficient is established.

### II. 1. FICK'S LAWS

Fick postulated that the flux across any given plane normal to the direction of matter flow is proportional to the concentration gradient across that plane. i.e.,

$$\vec{J} = -D \text{ grad } c \quad (2.1)$$

where  $D$  is the diffusion coefficient. The negative sign ensures that  $D$  is positive, since the flux  $\vec{J}$  is usually in the direction of decreasing concentration. Equation (2.1) is known as Fick's First Law of Diffusion.

$\vec{J}$  represents the net number of atoms of the diffusing species passing through unit area of the plane in unit time. Since  $J$  has the dimensions  $(\text{time-area})^{-1}$  and  $\nabla c$   $(\text{volume-length})^{-1}$ , the diffusion coefficient has the dimensions area/time. Usually,  $D$  is expressed in  $\text{cm}^2/\text{sec}$ .

If the concentration gradient is along an arbitrary direction, then the diffusion coefficient, with respect to an arbitrary set of coordinates  $(\alpha, \beta, \gamma)$  will be given by a tensor as

$$D = \begin{pmatrix} D_{\alpha\alpha} & D_{\alpha\beta} & D_{\alpha\gamma} \\ D_{\beta\alpha} & D_{\beta\beta} & D_{\beta\gamma} \\ D_{\gamma\alpha} & D_{\gamma\beta} & D_{\gamma\gamma} \end{pmatrix}$$



where the coefficient  $D_{mn}$  relates the flux in the direction  $m$  to the gradient of the concentration along the direction  $n$ .

If now, the principal axes of the crystal are chosen as the reference coordinates, then all the off-diagonal terms vanish and only the three coefficients  $D_{xx}$ ,  $D_{yy}$  and  $D_{zz}$  remain.

In the case of a cubic crystal, the three axes are equivalent and hence

$$D_{xx} = D_{yy} = D_{zz}.$$

A more useful expression can be obtained from equation (2.1) by the application of the law of conservation of matter; i.e.,

$$\frac{\partial c}{\partial t} = - \text{Div } \vec{J} \quad (2.2)$$

Using equation (2.1) in (2.2),

$$\frac{\partial c}{\partial t} = \text{Div } (D \text{ grad } c) \quad (2.3)$$

where, in the case of a cubic crystal,  $D$  is a constant.

If the concentration gradient is along one particular direction, say the  $x$  axis, then equation (2.3) becomes

$$\frac{\partial c}{\partial t} = \frac{\partial}{\partial x} \left( D \frac{\partial c}{\partial x} \right)$$

and finally, if the diffusion coefficient is independent of position, equation (2.3) reduces to

$$\frac{\partial c}{\partial t} = D \frac{\partial^2 c}{\partial x^2} \quad (2.4)$$

This differential equation is known as Fick's Second Law of Diffusion.

Equation (2.4) can be solved for  $c = c(x,t)$  for the particular set of initial and boundary conditions applicable to the present investigation (Appendix A). The solution is given as

$$c(x,t) = \frac{S_0}{\sqrt{\pi Dt}} \exp(-x^2/4Dt) \quad (2.5)$$

where  $S_0$  represents the total number of atoms whose diffusion is being studied and  $t$  is the time of the diffusion anneal.

Using equation (2.5), the diffusion coefficient can be extracted from the concentration-penetration profile of the data obtained in an experiment.

## II. 2. MACROSCOPIC CONSIDERATIONS

Using probability theory (18), it can be shown that the net flux  $J_x$  across any reference plane  $x_0$ , is given by

$$J_x = - \frac{\langle x^2 \rangle}{2t} \left( \frac{\partial c}{\partial x} \right) \quad (2.6)$$

where  $\langle x^2 \rangle$  is the mean square displacement along the  $x$  direction and  $x$  is a principal axis. Similar relationships hold when the concentration gradient is along the other principal axes  $y$  and  $z$ , that is

$$J_y = - \frac{\langle y^2 \rangle}{t} \frac{\partial c}{\partial y} \quad (2.7)$$

$$\text{and } J_z = \frac{\langle z^2 \rangle}{2t} \frac{\partial c}{\partial z} \quad (2.8)$$

From Fick's Law, the coefficients that relate the flux and the concentration gradient can be identified as

$$\left. \begin{aligned} D_x &= \frac{\langle x^2 \rangle}{2t} \\ D_y &= \frac{\langle y^2 \rangle}{2t} \\ D_z &= \frac{\langle z^2 \rangle}{2t} \end{aligned} \right\} \quad (2.9)$$

For a cubic crystal,  $D_x = D_y = D_z = D$ .

$$\text{Then, } D_x + D_y + D_z = 3D = \frac{\langle x^2 \rangle + \langle y^2 \rangle + \langle z^2 \rangle}{2t}$$

which gives

$$\langle R^2 \rangle = 6Dt \quad (2.10)$$

where  $\langle R^2 \rangle = \langle x^2 \rangle + \langle y^2 \rangle + \langle z^2 \rangle$  is the mean square displacement of the atoms during time  $t$ .

It is to be noted that in the derivation of equation (2.10), no particular model was assumed for the atomic jump mechanism.

### II. 3. RANDOM WALK

It is now well established that the atoms migrate through the lattice by a series of atomic jumps. Several models have been proposed, of which the single vacancy, divacancy, interstitial, interstitialcy, dislocations, etc. are examples.

The treatment of the atomic jumps has come to be called the "random walk problem" and a number of authors have discussed this (19,20,21).

To bring out the salient points of the random walk treatment, the single vacancy mechanism is taken to be operative in the following.

It is assumed that the  $k$ th atom starting from the origin makes a series of jumps by exchanging positions with near neighbor vacancies. If the total number of jumps made by this  $k$ th atom in time  $t$  is  $n_k$ , the resultant displacement is given by

$$\underline{R}_k = \sum_{i=1}^{n_k} \underline{r}_{ik} \quad (2.11)$$

where the  $\underline{r}_{ik}$  are vectors representing the individual jumps. Then

$$R_k^2 = \sum_{i=1}^{n_k} r_{ik}^2 + 2 \sum_{j=1}^{n_k-1} \sum_{i=1}^{n_k-j} (\underline{r}_i \cdot \underline{r}_{i+j})_k \quad (2.12)$$

For crystals with cubic symmetry, all the jump vectors will be equal in magnitude, and equation (2.12) can be rewritten as

$$R_k^2 = n_k r^2 \left[ 1 + \frac{2}{n_k} \sum_{j=1}^{n_k-1} \sum_{i=1}^{n_k-j} \cos \theta_{i,i+j} \right]_k \quad (2.13)$$

where  $\theta_{i,i+j}$  is the angle between two vectors separated by  $j$  jumps, and  $\underline{r}$  is the jump distance.

To obtain the value of  $\langle R^2 \rangle$ , a large number of atoms have to be considered. Assuming an average value  $\bar{n}$  of jumps, equation (2.13) can be rewritten as

$$\langle R^2 \rangle = \bar{n} r^2 \left[ 1 + \frac{2}{\bar{n}} \sum_{j=1}^{\bar{n}-1} \sum_{i=1}^{\bar{n}-j} \overline{\cos \theta_{i,i+j}} \right] \quad (2.14)$$

Now, if the directions of the jumps are random, positive and negative values of any given  $\cos \theta_{i,i+j}$  will occur with equal frequency, thus reducing the average value of the double sum to zero. However, for several of the atomic jump models, the successive jumps are not random. In the present case of diffusion via vacancy mechanism in a cubic lattice, after any jump of the atom, all of its neighbors are not identical; one of them is a vacancy and the most probable next jump direction for the atom is back towards the vacancy. The direction of a jump is thus related to the direction of the previous jump. Successive atomic jumps, in such a case, are said to be "correlated", and a measure of the correlation is given by the

"correlation factor", usually denoted by 'f'.

The correlation factor can be calculated theoretically if the jump mechanism and the structure of the lattice are known (22,23).

When the atomic jumps are correlated, equation (2.14) takes the form

$$\langle R^2 \rangle = \bar{n} \gamma^2 f \quad (2.15)$$

where the correlation factor f is given by

$$f = \lim_{\bar{n}, t \rightarrow \infty} \left[ 1 + \frac{2}{\bar{n}} \sum_{j=1}^{\bar{n}-1} \sum_{i=1}^{\bar{n}-j} \overline{\cos \theta_{i,i+j}} \right]$$

Combining equations (2.15) and (2.10), an expression for the diffusion coefficient can be obtained as

$$D = \frac{1}{6} \Gamma \gamma^2 f \quad (2.16)$$

where  $\Gamma = \lim_{\bar{n}, t \rightarrow \infty} \frac{\bar{n}}{t}$ , defines the average atomic jump frequency.

In the case of interstitial diffusion, however, there is no correlation between successive jumps, and the double sum in expression (2.14) vanishes; the value of the correlation factor reduces to unity and the expression for the diffusion coefficient becomes

$$D = \frac{1}{6} \Gamma \gamma^2$$

which is a special case of the equation (2.16).

## II. 4. TEMPERATURE DEPENDENCE OF THE DIFFUSION COEFFICIENT.

The atoms in a crystal execute small oscillations about their equilibrium positions. Although the vibrational amplitude of an

atom remains small most of the time, occasionally, the atom acquires enough energy due to local thermal fluctuations, resulting in a large amplitude. This extra energy carries the atom from an initial equilibrium position to one of the lattice sites in its first coordination shell, over the potential barrier. The atomic jump frequency is, therefore, a product of two factors: the vibration frequency of the atom and the probability that a fluctuation exists that gives the atom an energy greater than  $\Delta g^m$ , this being the difference in the Gibbs free energy between the saddle point and an equilibrium position.

$$\text{i.e., } \Gamma = \nu p$$

Here  $\nu$  is the effective vibration frequency of the atom; this has to be defined because of a wide frequency spectrum of the atoms. The factor  $p$  represents the probability that the atom has enough energy to make the jump.

Thus,  $\Gamma$  has a Boltzmann dependence on temperature and the probability  $p$  can be written as

$$p = \exp(-\Delta g^m / kT)$$

where  $k$  is the Boltzmann's constant.

In the simplest case of interstitial diffusion, the expression for the jump frequency is simply

$$\Gamma = \nu \exp(-\Delta g^m / kT)$$

Substituting this in the expression (2.16), the diffusion coefficient is given as

$$D = D_0 \exp(-Q / kT)$$

where

$$D_0 = \frac{r^2 f \nu}{6} \exp(\Delta S^m / R)$$

and

$$Q = \Delta H^m$$

Here  $\Delta g^m = \Delta h^m - T\Delta s^m$ ,  $\Delta h^m$  and  $\Delta s^m$  being the changes in enthalpy and entropy, respectively.

In the case of diffusion via the single vacancy mechanism, a jump frequency  $\omega$  can be associated with the vacancy and the atomic jump frequency can be expressed as

$$\Gamma = p_v p_j$$

where  $p_v$  represents the probability that a site is vacant and  $p_j$  is the probability that the atom is going to exchange place with the vacancy.

The probability  $p_v$  is a product of the vacancy concentration ( $n/N$ ) and the coordination number  $z$ ,  $n$  and  $N$  representing the total number of vacancies and the atoms, respectively. The vacancy concentration can be obtained from statistical thermodynamics by minimizing the Gibbs free energy less the configurational entropy as

$$(n/N) \approx \exp(-\Delta g^f / kT)$$

where  $\Delta g^f$  is the increase in the Gibbs free energy of the crystal due to the formation of the vacancy;  $\Delta g^f = \Delta h^f - T\Delta s^f$ ,  $\Delta h^f$  and  $\Delta s^f$  being the changes in the enthalpy and entropy respectively.

The probability  $p_j$  is given as the ratio of the vacancy jump frequency to the number of first nearest neighbors;

$$p_j = (\omega / z)$$

where

$$\omega = \nu \exp(-\Delta g^m / kT)$$

The atomic jump frequency  $\Gamma$  with the expressions for

$p_v$  and  $p_j$  becomes

$$\Gamma = \nu \exp [-(\Delta g^f + \Delta g^m)/kT]$$

This is consistent with the observation that the total number of atomic jumps equals the total number of vacancy jumps, if the vacancy mechanism alone is operative.

The expression for the diffusion coefficient is

$$D = D_0 \exp(-Q/kT)$$

where, now

$$D_0 = \frac{r^2 f \nu}{6} \exp [(\Delta h^f + \Delta h^m)/kT]$$

and

$$Q = \Delta h^f + \Delta h^m$$

Thus, the diffusion coefficient has a temperature dependence expressed as

$$D = D_0 \exp(-Q/kT)$$

when a single mechanism is operative, with the frequency factor  $D_0$  and the activation energy  $Q$  appropriately defined.

In the case of self diffusion, the correlation factor  $f$  is independent of temperature; the temperature dependence of  $D$  therefore comes only from the jump frequency  $\Gamma$ . For impurity diffusion, however, the correlation factor is not temperature independent; the temperature dependence of  $D$  thus comes from both  $\Gamma$  and  $f$ , the latter usually being small in magnitude (24).



### CHAPTER III. EXPERIMENTAL TECHNIQUE

A thin film of radioactive substance whose diffusion is being studied, is evaporated on a plane surface of the specimen. The specimen is annealed at an elevated temperature for a known time  $t$ . On subsequent cooling, thin sections parallel to the face of the specimen are removed, accurately weighed and the relative concentration of the tracer in these sections determined.

The appropriate solution of the Fick's equation under these conditions (Appendix A) is given by

$$C(x,t) = \frac{S_0}{\sqrt{\pi Dt}} \exp(-x^2/4Dt)$$

where  $S_0$  is the amount of tracer initially deposited on the face.

Thus, from the data collected, a plot of the log concentration versus the square of the penetration distance can be drawn, the slope of which gives  $(4Dt)^{-1}$ ; from this the diffusion coefficient can be extracted, given the measured time of anneal  $t$ .

Section 3 describes the preparation of the specimen, section 4 the evaporation of the tracer and section 5, the actual diffusion anneal. Sections 6 and 7, deal with the lathe-sectioning and the measurement of the specific activity respectively, while section 8 shows the method of extracting the diffusion coefficient from the concentration profile.

The calibration of the  $W-Re$  thermocouple is described in section 2; section 1 describes the functioning of the temperature controller/recorder assembly.

### III. 1. TEMPERATURE CONTROLLER/RECORDER ASSEMBLY

To record the voltage output of the thermocouple, a modified form of Texas Instrument Flushmount Recorder Model No. 185000-9701 [Plate 2] was used. This has two recording scales, one with a full scale deflection of 50 millivolts, the other with a center zero and a full scale deflection of 1 millivolt. The former directly records the voltage generated by the thermocouple while the latter records the deviation of this voltage from a preset potential (bucking potential).

By selecting the bucking potential equal but in opposition to the e.m.f. generated by the thermocouple at the desired annealing temperature, the difference voltage was monitored on the second recorder scales. The movement of the pen activated two microswitches on each side of the zero line which in turn controlled the on-off operation of a "topping" voltage superimposed on a base voltage supply to the furnace. With this arrangement, temperatures were controlled to within  $\pm 1^{\circ}\text{C}$ .

### III. 2. CALIBRATION OF THE THERMOCOUPLE

The calibration of the  $\text{W-Re}$  thermocouple was done by measuring the e.m.f. generated at the melting points of gold and platinum.

A small length of gold (99.999% purity) wire was wrapped around the thermocouple hot junction, while the cold junction was kept immersed in an ice-bath. The bucking potential of the flushmount recorder was set at a value 0.1 millivolt higher than that corresponding to the melting temperature of gold ( $1063^{\circ}\text{C}$ ). The speed of the chart

were usually set at 2"/minute.

The "thermal arrest" during the heating or cooling was observed on the time-voltage record. Due to surface tension effects, the molten wire clung to the thermocouple, permitting repeated observations of the thermal arrest.

For gold, the thermal arrest was observed three times; for platinum (99.9999% purity), the heating and cooling were done only once. The results of the calibration measurements are given in Chapter IV.

### III. 3. PREPARATION OF THE SPECIMENS

The Zirconium and Titanium, used in the preparation of the  $\text{Zr}_{50}\text{Ti}_{50}$  alloy<sup>†</sup>, were obtained from the Foote Mineral Company, Exton, Pennsylvania, U.S.A. The chemical analysis of zirconium, as given by the supplier, is shown in Table III. 1., the titanium was 99.9% pure.

<sup>†</sup> Some of the specimens were prepared and tracer evaporated on one face at Chalk River Nuclear Laboratories, Chalk River, Ontario.

ELEMENT	PERCENTAGE
Zr (by difference)	99.91
Sn	0.003
Si	0.005
Al	0.002
Mg	0.005
Fe	0.001
Ti	0.001
Ni	0.002
Ca	0.002
Cu	0.0003

TABLE III. 1. CHEMICAL ANALYSIS OF ZIRCONIUM

The two metals were melted in a cold hearth arc furnace under an atmosphere of Argon. The resulting ingots were swaged to produce rods of approximately  $9\frac{1}{2}$  mms. in diameter. These rods were then cut into sections, approximately  $6\frac{1}{2}$  mms. in length. The faces were ground and chemically polished using a 50% by volume  $H_2O$ , 45%  $HNO_3$  and 5% HF solution.

After the chemical polishing, the specimens were encapsulated in a zirconium tube, two at a time, and preannealed at  $1000^\circ C$  for 50-70 hours under a vacuum of  $1 \times 10^{-5}$  mms. of Hg, to ensure homogeneity.

### III. 4. EVAPORATION OF TRACER

The radioactive tracer isotope  $\text{Co}^{60}$  was prepared by neutron irradiation of 99.999% pure cobalt wire in the McMaster nuclear reactor. Small rings were placed in a crucible-like tungsten filament and a current of approximately 20 amperes was passed through the filament to melt and then vaporise the cobalt; the emitted vapor condensed on to the surfaces of the specimens surrounding the source.

No special care was taken to get a uniform layer, as non-uniformity in the film does not affect the value of the diffusion coefficient (25).

The arrangement of the specimens for the tracer evaporation is shown in Plate 1.

### III. 5. DIFFUSION ANNEAL

For each run, a specimen was placed in a small zirconium container, inside a tantalum furnace tube. The specimen was isolated from the container by tungsten wires in order to prevent welding at the elevated temperatures.

After a vacuum of  $10^{-5}$  mms. of Hg or better was reached, the furnace tube was rapidly heated by passing a power of about 1000 volt-amperes via a step-down transformer and through the tube. Temperatures as high as  $1600^{\circ}\text{C}$  could be reached within two minutes, using this furnace. A schematic diagram of the heating circuit is shown in fig. III. 1.

Temperatures were controlled and recorded by the Flushmount Controller/Recorder Assembly, described in section III. 1.

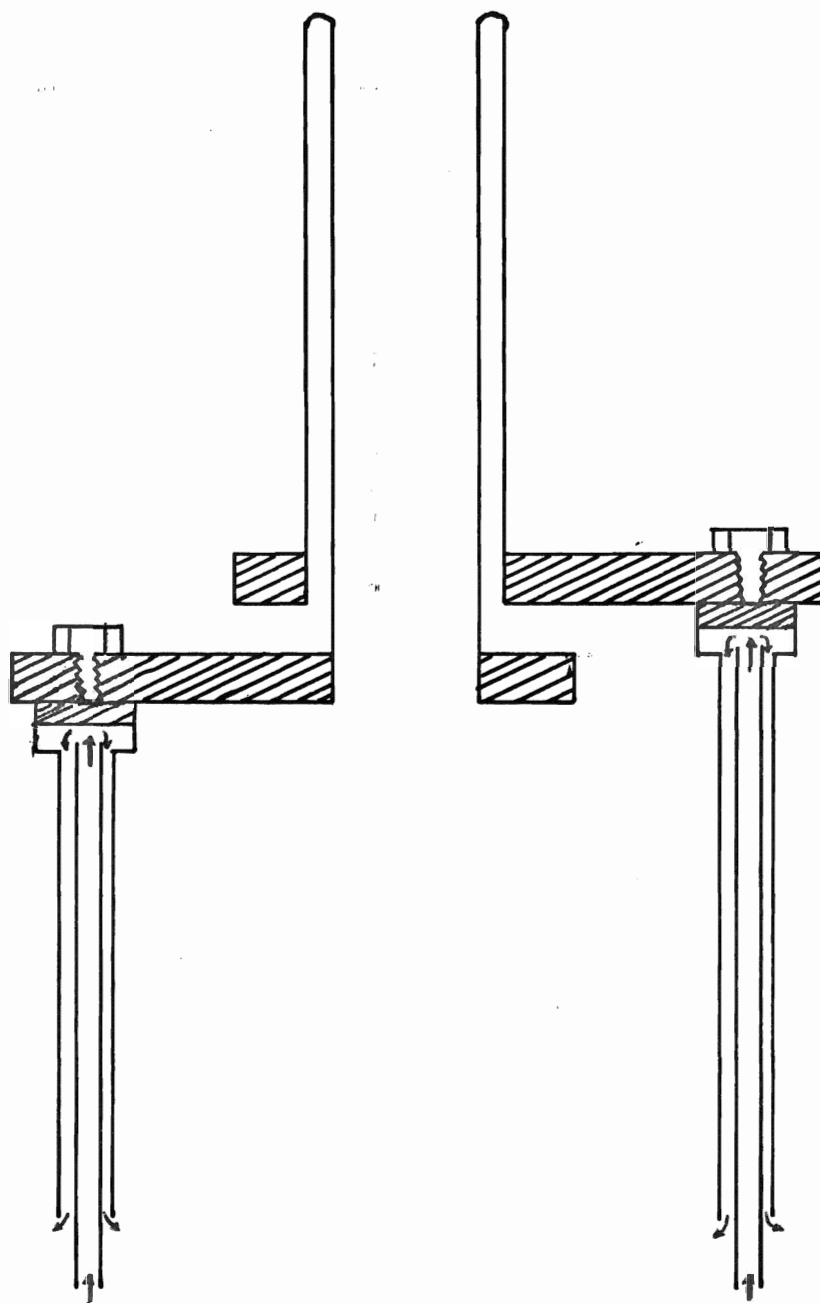


Fig. III.1. The Heating Circuit.

### III. 6. SECTIONING METHOD

Sectioning was performed on a precision lathe. The diffusion annealed specimen was mounted on a chuck designed to permit a wide adjustment of the specimen orientation relative to the lathe axis. The alignment was checked with a dial indicator in contact with the specimen surface. After the specimen surface was oriented at right angles to the lathe axis, a thickness of six to eight times the estimated value of  $(Dt)^{1/2}$  was removed from the sides of the specimen, to eliminate effects due to surface diffusion (26). The final cross-sectional area was accurately measured with a micrometer.

Sectioning was performed by an appropriate cutting tool, suited for the material [Plate 3]. In order to maintain a near-uniform counting rate, the thickness of the section was increased with increasing depth in the specimen. A total length of about 2500 microns was usually removed. In some cases, deeply penetrating tails were observed; in such cases, more sections beyond the usual range of 2500 microns were taken. The sections were collected in a set of pre-weighed bottles attached to a specially designed funnel (shown in Plate 4) and the weights determined as the difference between the weights of the bottle with the sections less those of the bottles to an accuracy of 10  $\mu$ gm. Section thicknesses were calculated from the measured section weights, the measured cross-sectional area of the specimen and the known density of the alloy (5.63 gm/cc).

The penetration distances were subsequently calculated from the thicknesses. The midpoint distance  $x_n$  of the  $n^{\text{th}}$  section from

the face  $x = 0$ , for example, is given by

$$X_n = \left( \sum_{i=1}^{n-1} t_i \right) + \frac{t_n}{2}$$

where  $t_i$  represents the thickness of the  $i^{\text{th}}$  section.

### III. 7. MEASUREMENT OF SPECIFIC ACTIVITY

After dissolving the sections in a 50%  $\text{H}_2\text{O}$ , 45%  $\text{HNO}_3$  and 5%  $\text{HF}$  solution, the activity of  $\text{Co}^{60}$  associated with the two photopeaks of energy 1.17 Mev and 1.33 Mev was counted in a well-type NaI (Tl) scintillation counter.

The electronics and the procedure used for discriminating the two  $\text{Co}^{60}$  photopeaks from the full spectrum and subsequent counting are described in detail in Appendix B.

A total of 10,000 pulses were counted in order to keep the statistical error in counting within 1%.

The specific activities were calculated from the measured total activity of each section, the average background counts, and the weight of each section. To correct for the decay time, each specific activity was then divided by the activity of a section chosen as the "standard". These ratios are, then, directly proportional to the concentration of the diffusant in the sections.

### III. 8. DIFFUSION COEFFICIENT

From the measured tracer concentration of the sections and the weights of the sections, the specific activities and the penetration distance squared could be calculated. A least squares fit analysis



would then give the slope of the log specific activity versus penetration distance squared graph. The Wang 700 calculator was programmed to carry out the calculations and a sample output is shown in pages 30-39.

The diffusion coefficient could be calculated from the slope of the log specific activity versus penetration distance squared graph, with the known annealing time  $t$ . A first-order correction to the annealing time, however, becomes necessary; this correction can be obtained using the relation

$$t_{\text{eff}} = \frac{1}{D_{\text{eff}}} \int_0^t D(t) dt$$

where  $t_{\text{eff}}$  is the effective time for diffusion at a temperature  $T_0$  and  $D_{\text{eff}} = D(T_0)$ . Here, the area of the actual  $D$  versus  $t$  curve is equated to the area of a rectangular curve of height  $D(T_0)$  and breadth  $t_{\text{eff}}$ , to give the desired time-correction.

Results of the various runs are given in Chapter IV.

DIFFUSION OF COBALT IN ZIRCONIUM - TITANIUM ALLOY

R # 30.1.1973.

Temperature of Anneal = 900°C.

CONVERSION FACTOR CALCULATION

Surface : Circular (00)  
          Rectangular (01)  
          Triangulation (02)

CIRCULAR       $r(\text{cm}) = .3780$        $\text{AREA } .4488(\text{cm})^{**2}$   
                  $\text{density} = 5.6300(\text{gm})/(\text{cm})^{**3}$   
  
                  $\text{conversion factor} = .3956(\text{cm})/(\text{gm})$

THE CALCULATION OF TRACER PENETRATION DISTANCE SQUARED

KEY IN NO. OF MASSES      PRESS GO      N = 40

KEY IN MASS in mgm.      PRESS GO

REPEAT STEP 2 FOR ALL MASSES

CONVERSION FACTOR = .395692736184ex 00

SECTION #	MASS	PEN. DIST.	PEN. DIST. SQ'D
1	4.97	.983296573665ex-03	.966872151781ex-06
2	5.04	.296373896851ex-02	.878374367346ex-05
3	5.85	.511828618927ex-02	.261968535152ex-04
4	5.94	.745089516381ex-02	.555158387420ex-04
5	5.14	.964303319926ex-02	.929880892820ex-04
6	6.75	.119954268130ex-01	.143890264426ex-03
7	5.56	.144309159118ex-01	.208251334053ex-03
8	6.03	.167239556076ex-01	.279690691164ex-03
9	3.34	.185777763108ex-01	.345133772654ex-03
10	5.75	.203762000239ex-01	.415189527413ex-03
11	10.76	.236426439737ex-01	.558974614067ex-03
12	12.00	.281456278804ex-01	.792176368781ex-03
13	12.06	.329058120981ex-01	.108279246983ex-02
14	11.86	.376382978207ex-01	.141664146283ex-02
15	12.54	.424657498120ex-01	.180333990709ex-02
16	10.89	.471012908020ex-01	.221853159521ex-02
17	11.62	.515548131104ex-01	.265789875484ex-02
18	13.22	.564693175147ex-01	.318878382057ex-02
19	11.78	.614154773419ex-01	.377186085713ex-02
20	11.54	.660292552287ex-01	.435986254605ex-02
21	18.30	.719329915984ex-01	.517435528029ex-02
22	18.46	.792058250083ex-01	.627356271524ex-02
23	16.60	.861423195500ex-01	.742049921745ex-02
24	18.94	.931737803604ex-01	.868135334664ex-02
25	19.74	.100826478845ex-00	.101659788362ex-01
26	18.87	.108465328081ex-00	.117647273957ex-01
27	16.20	.115403801086ex-00	.133180373050ex-01
28	18.18	.122205760080ex-00	.149342477967ex-01
29	19.68	.129696224522ex-00	.168211106552ex-01
30	17.28	.137008627210ex-00	.187713639299ex-01
31	22.63	.144904676757ex-00	.209973653460ex-01
32	25.84	.154494291429ex-00	.238684860841ex-01
33	25.96	.164742734590ex-00	.271401686001ex-01
34	23.66	.174559872614ex-00	.304711491270ex-01
35	27.95	.184770724960ex-00	.341402208022ex-01
36	22.97	.194845063295ex-00	.379645986904ex-01
37	24.75	.204286293173ex-00	.417328895783ex-01

38	27.21	.214566391758ex-00	.460387364720ex-01
39	24.00	.224698105548ex-00	.504892386368ex-01
40	27.51	.234889173255ex-00	.551729237124ex-01

SET EXPONENT = -1

# THE CALCULATION OF THE LOG CONCENTRATION RATIO OF TRACER

N = 5

BKG(I) =	1.760 cts/sec	T(M.P.) =	50.00 sec
BKG(F) =	1.950 cts/sec	T(M.P.) =	450.00 sec
STD(I) =	3225.806 cts/sec	T(M.P.) =	136.55 sec
STD(F) =	3225.806 cts/sec	T(M.P.) =	536.55 sec

SPC.NO.	MASS(mgm)	T(M.P.)	SPC.ACT.	R	LN(R)
1	4.97	151.55	3225.80	.201207243460ex 00	-.160341984011ex 01
2	5.04	212.40	2083.33	.128101491216ex-00	-.205493242911ex 01
3	5.85	257.10	2380.95	.126144319482ex-00	-.207032863478ex 01
4	5.94	297.15	2325.58	.121341367233ex-00	-.210914748874ex 01
5	5.14	337.40	2083.33	.125607974571ex-00	-.207458953515ex 01

N = 5

BKG(I) =	1.950 cts/sec	T(M.P.) =	450.00 sec
BKG(F) =	1.870 cts/sec	T(M.P.) =	825.00 sec
STD(I) =	3225.806 cts/sec	T(M.P.) =	536.55 sec
STD(F) =	3225.806 cts/sec	T(M.P.) =	911.55 sec

SPC.NO.	MASS (mgm)	T(M.P.)	SPC.ACT.	R	LN(R)
6	6.75	575.95	2564.10	.117740656375ex-00	-.213927090061ex 01
7	5.56	612.30	2173.91	.121172537574ex-00	-.211053981869ex 01
8	6.03	651.25	2222.22	.114213076965ex-00	-.216968947899ex 01
9	3.34	694.00	1250.00	.115910004557ex-00	-.215494121176ex 01
10	5.75	737.45	2040.81	.109989192569ex-00	-.220737316739ex 01

N = 5

BKG(I) =	1.870 cts/sec	T(M.P.) =	825.00 sec
BKG(F) =	2.010 cts/sec	T(M.P.) =	1185.00 sec
STD(I) =	3225.806 cts/sec	T(M.P.) =	911.55 sec
STD(F) =	3125.000 cts/sec	T(M.P.) =	1266.60 sec

SPC.NO.	MASS (mgm)	T(M.P.)	SPC.ACT.	R	LN(R)
11	10.76	941.40	3571.42	.103171453571ex-00	-.227136307688ex 01
12	12.00	981.35	3703.70	.962782460000ex-01	-.234051288392ex 01
13	12.06	1016.45	3448.27	.894672589079ex-01	-.241388254286ex 01
14	11.86	1056.65	3030.30	.802290370503ex-01	-.252286977165ex 01
15	12.54	1091.85	2702.70	.678832223544ex-01	-.268996636839ex 01

N = 5

BKG(I) =	2.010 cts/sec	T(M.P.) =	1185.00 sec
BKG(F) =	2.120 cts/sec	T(M.P.) =	1540.00 sec
STD(I) =	3125.000 cts/sec	T(M.P.) =	1266.60 sec
STD(F) =	3225.806 cts/sec	T(M.P.) =	1636.55 sec

SPC.NO.	MASS (mgm)	T(M.P.)	SPC.ACT.	R	LN(R)
16	10.89	1302.40	2083.33	.610076191660ex-01	-.279675651824ex 01
17	11.62	1342.50	2000.00	.546948108934ex-01	-.290598643887ex 01
18	13.22	1377.65	1886.79	.452132666204ex-01	-.309636472590ex 01
19	11.78	1413.50	1428.57	.382852642742ex-01	-.326269020161ex 01
20	11.54	1449.25	1176.47	.320757181158ex-01	-.343965598007ex 01

N = 5

BKG(I) = 2.120 cts/sec T(M.P.) = 1540.00 sec  
 BKG(F) = 1.860 cts/sec T(M.P.) = 2930.00 sec  
 STD(I) = 3225.806 cts/sec T(M.P.) = 1636.55 sec  
 STD(F) = 3225.806 cts/sec T(M.P.) = 3141.55 sec

SPC.NO.	MASS(mgm)	T(M.P.)	SPC.ACT.	R	LN(R)
21	18.30	1678.60	1388.88	.235074127350ex-01	-.375043947202ex 01
22	18.46	1734.95	1010.10	.169386446838ex-01	-.407815759981ex 01
23	16.60	2012.95	628.93	.117145328145ex-01	-.444692508706ex 01
24	18.94	2070.25	487.80	.795604317286ex-02	-.483382349154ex 01
25	19.74	2135.05	332.22	.518901322061ex-02	-.526121173077ex 01

N = 5

BKG(I) = 1.860 cts/sec T(M.P.) = 2930.00 sec  
 BKG(F) = 2.010 cts/sec T(M.P.) = 4350.00 sec  
 STD(I) = 3225.806 cts/sec T(M.P.) = 3141.55 sec  
 STD(F) = 3225.806 cts/sec T(M.P.) = 4736.55 sec

SPC.NO.	MASS(mgm)	T(M.P.)	SPC.ACT.	R	LN(R)
26	18.87	3199.75	202.02	.328972820935ex-02	-.571695032875ex 01
27	16.20	3305.00	111.11	.209108105707ex-02	-.617007409453ex 01
28	18.18	3446.30	88.80	.148259480798ex-02	-.651396147771ex 01
29	19.68	3905.50	58.47	.890791617596ex-03	-.702340003258ex 01
30	17.28	4144.10	41.98	.717914495428ex-03	-.723916008313ex 01

N = 5

BKG(I) = 2.010 cts/sec    T(M.P.) = 4350.00 sec  
 BKG(F) = 1.600 cts/sec    T(M.P.) = 7970.00 sec  
 STD(I) = 3225.806 cts/sec    T(M.P.) = 4736.55 sec  
 STD(F) = 3225.806 cts/sec    T(M.P.) = 8321.55 sec

SPC.NO.	MASS(mgm)	T(M.P.)	SPC.ACT.	R	LN(R)
31	22.63	4923.55	32.56	.419672817437ex-03	-.777603515635ex 01
32	25.84	5263.70	33.62	.380745627322ex-03	-.787337905063ex 01
33	25.96	6582.10	26.72	.298298473057ex-03	-.811741598526ex 01
34	23.66	7087.45	17.39	.205740517192ex-03	-.848889480843ex 01
35	27.95	7651.00	26.88	.280146852081ex-03	-.818019662055ex 01

N = 5

BKG(I) = 1.600 cts/sec    T(M.P.) = 7970.00 sec  
 BKG(F) = 1.740 cts/sec    T(M.P.) = 13160.00 sec  
 STD(I) = 3225.806 cts/sec    T(M.P.) = 8321.55 sec  
 STD(F) = 3225.806 cts/sec    T(M.P.) = 13246.55 sec

SPC.NO.	MASS(mgm)	T(M.P.)	SPC.ACT.	R	LN(R)
36	22.97	8749.15	13.54	.161000353416ex-03	-.873410399784ex 01
37	24.75	10571.95	13.81	.152183898463ex-03	-.879042091009ex 01
38	27.21	11330.25	16.11	.164432808679ex-03	-.871300852907ex 01
39	24.00	11922.00	19.08	.224576435836ex-03	-.840129443729ex 01
40	27.51	12609.95	12.82	.125114829312ex-03	-.898627860784ex 01

PLOT OF LN(R) VS XSQ

DELTA LN(R) = .107834400000ex-00  
 DELTA XSQ = .788171428571ex-03

```

.....
* P( 1)
* P( 2)
* P( 3)
* P( 4)
* P( 5)
* P( 6)
* P( 7)
* P( 8)
* P( 9)
* P(10)
* P(11)
* P(12)
* P(13)
* P(14)
* P(15)
* P(16)
* P(17)
* P(18)
* P(19)
* P(20)
* P(21)
* P(22)
* P(23)
* P(24)
* P(25)
* P(26)
* P(27)
* P(28)

```



.....

\* P( 29)

\* P( 30)

\* P( 31)

\* P( 32)

\* P( 33)

\* P( 34)

\* P( 35)

\* P( 36)

\* P( 37)

\* P( 38)

\* P( 39)

\* P( 40)

DATA EDIT PROGRAM

Points Deleted	1	26	27	28
	29	30	31	32
	33	34	35	36
	37	38	39	40

DIFFUSION COEFFICIENT CALCULATION

anneal temp = 900°C  
anneal time = .729245000000ex 04 sec.

Least Squares Analysis

Ln C	X SQ
-2.054932	.870000000000ex-05
-2.070328	.261000000000ex-04
-2.109147	.555000000000ex-04
-2.074589	.929000000000ex-04
-2.139270	.143800000000ex-03
-2.110539	.208200000000ex-03
-2.169689	.279600000000ex-03
-2.154941	.345100000000ex-03

-2.207373	.415100000000ex-03
-2.271363	.558900000000ex-03
-2.340512	.792100000000ex-03
-2.413880	.108270000000ex-02
-2.522860	.141660000000ex-02
-2.689960	.180330000000ex-02
-2.796750	.221850000000ex-02
-2.905980	.265780000000ex-02
-3.096360	.318870000000ex-02
-3.262690	.377180000000ex-02
-3.439650	.435980000000ex-02
-3.750430	.517430000000ex-02
-4.078150	.627350000000ex-02
-4.446920	.742040000000ex-02
-4.833820	.868130000000ex-02
-5.261200	.101659000000ex-01

slope = -317.363281288

cor. fact. = -.999745809036ex 00

DIF. COEF'T = .108021417213ex-06  $\pm$  .385174685644ex-09 cm<sup>2</sup>/sec.

## CHAPTER IV. RESULTS

## IV. 1. CALIBRATION OF THE THERMOCOUPLE

The results of the calibration of the W-Re thermocouple are shown in figure 4.1 for gold and in figure 4.2 for platinum.

In order to determine the melting temperature  $T_m$  of gold (1063°C or 19.325 mVs), the bucking potential of the recorder was set at 19.425 mVs, about tenth of a millivolt away from the melting point, so that the thermal arrest during the heating or cooling could be observed 0.1 millivolt away from the set point. The chart speed was 2"/minute. In figure 4.1, the potential at which the thermal arrest began reads 19.229 millivolts, which corresponds to a temperature of 1058.0°C. The  $T_m$  of gold had thus been determined within -5.0°C, using the W-Re thermocouple.

To determine the melting temperature of platinum (1769°C or 30.675 mVs), the bucking potential was set at 30.850 mVs. From figure 4.2, the potential at which the thermal arrest began reads 30.710 mVs, which corresponds to 1771.2°C, on the temperature scale. Thus, the  $T_m$  of platinum had been determined within +2.2°C. However, due to the slow chart speed (1"/minute), there is an uncertainty of about 3°C in the temperature measurement. The results of the calibration runs are listed in Table IV. 1.

METAL	MEASURED VOLTAGE mVs.	CORRESPONDING TEMPERATURE °C	MELTING TEMPERATURE °C	DEVIATION °C
Gold	19.229	1058.0	1063	-5.0
Platinum	30.710	1771.2	1769	+2.2

TABLE IV. 1. Calibration of W-Re thermocouple

From Table IV. 1., it can be concluded that any error in the temperature measurements should be within about 5°C.

#### IV. 2. DIFFUSION MEASUREMENTS

Diffusion runs were done at 900°C, 1200°C and 1440°C. The concentration-penetration profiles obtained for the runs are shown in figures 4.3 to 4.8 and the various parameters are summarized in Table IV. 2. On several occasions, deeply penetrating tails were observed; these are shown on a reduced scale in boxes on the same graphs. In some cases, a second anomaly in the shape of the penetration profiles was observed. It is characterized by an unusually high initial point followed by a sharp dip, with a subsequent rise to join the normal linear region of the log concentration versus penetration distance squared curves. This has been reported and accounted for in terms of back diffusion (16,27).

In figures 4.3 to 4.8, points which have not been included in the least squares program for calculation of the slope, have been darkened.

#### IV. 3. PREANNEALING EXPERIMENTS

As mentioned previously (chapter I), the intent of the present investigation was to study the effect of prolonged preannealing of the specimen prior to the deposition of the tracer on the resultant diffusion coefficient. This was done using a specially designed apparatus shown in Plates 6 and 7.

RUN #	TEMP °C	ANNEAL TIME (secs)	SLOPE	DIFFUSION COEFFICIENT cm <sup>2</sup> /sec
21.8.'72	900	7183.29	-175.357	1.985ex-07 ± 1.236ex-09 *#
23.8.'72	900	7188.69	-168.960	2.058ex-07 ± 5.708ex-10
6.9.'72	1200	4843.70	-31.962	1.618ex-06 ± 6.727ex-09
7.10.'72	1200	4870.07	-32.323	1.588ex-06 ± 8.384ex-09
12.10.'72	1440	1466.78	-36.003	4.734ex-06 ± 2.866ex-08
27.2.'73	1440	1452.52	-46.247	3.722ex-06 ± 1.231ex-08 #
30.1.'73	900	7292.45	-317.363	1.080ex-07 ± 4.973ex-10

\* Errors include only those from the least squares fit analysis.

# Specimen prepared at Chalk River Nuclear Labs, Ontario, Canada.

TABLE IV.2. PARAMETERS USED IN DIFFUSION RUNS.

A carefully prepared specimen was annealed for  $4\frac{1}{2}$  hours. The specimen was then brought to the annealing temperature of  $900^{\circ}\text{C}$  and while maintaining the temperature at  $900^{\circ}\text{C}$ , the molybdenum radiation cover was raised and swung out of the way and the filament carrying the radioactive tracer lowered into the furnace tube. A thin layer of radioactive cobalt was evaporated from the filament on to the specimen, the radiation cover replaced and the diffusion anneal completed.

Table IV. 3. describes the thermal history of the specimen prior to the deposition of the tracer.

TEMPERATURE OF ANNEAL $^{\circ}\text{C}$	TIME OF ANNEAL (Mins)
1581	30
1392	30
1581	30
1392	30
1581	30
1392	30
1581	30
1392	30
1581	30
900	$17\frac{1}{2}$

TABLE IV. 3. THERMAL HISTORY OF SPECIMEN PRIOR TO TRACER DEPOSITION

The penetration profile resulting from this run, with a linear curve of larger slope and a long tail with a smaller slope, is shown in figure 4.9; the linear portion with the larger slope is shown on a larger scale in figure 4.10, in order to compare the slope with those of previous runs at the same annealing temperature. The analysis of this curve gives a diffusion coefficient which is less by a factor of two from that obtained in a conventional run, in which the tracer is evaporated at the room temperature and the specimen brought to the annealing temperature through the  $\alpha \rightarrow \beta$  phase transformation.

The Wang 700 calculator was programmed to carry out the calculations and a sample output shown in pages ( 30 - 39 ). The results of the present investigation and those of an earlier measurement (17) are shown in figure 4.14.

Figures 4.11, 4.12 and 4.13 include the slopes of the diffusion runs to show the reproducibility of data, using the sectioning technique. Fig. 4.11 is particularly noteworthy, as it exhibits the effect of the preannealing on the slope of the penetration profile.



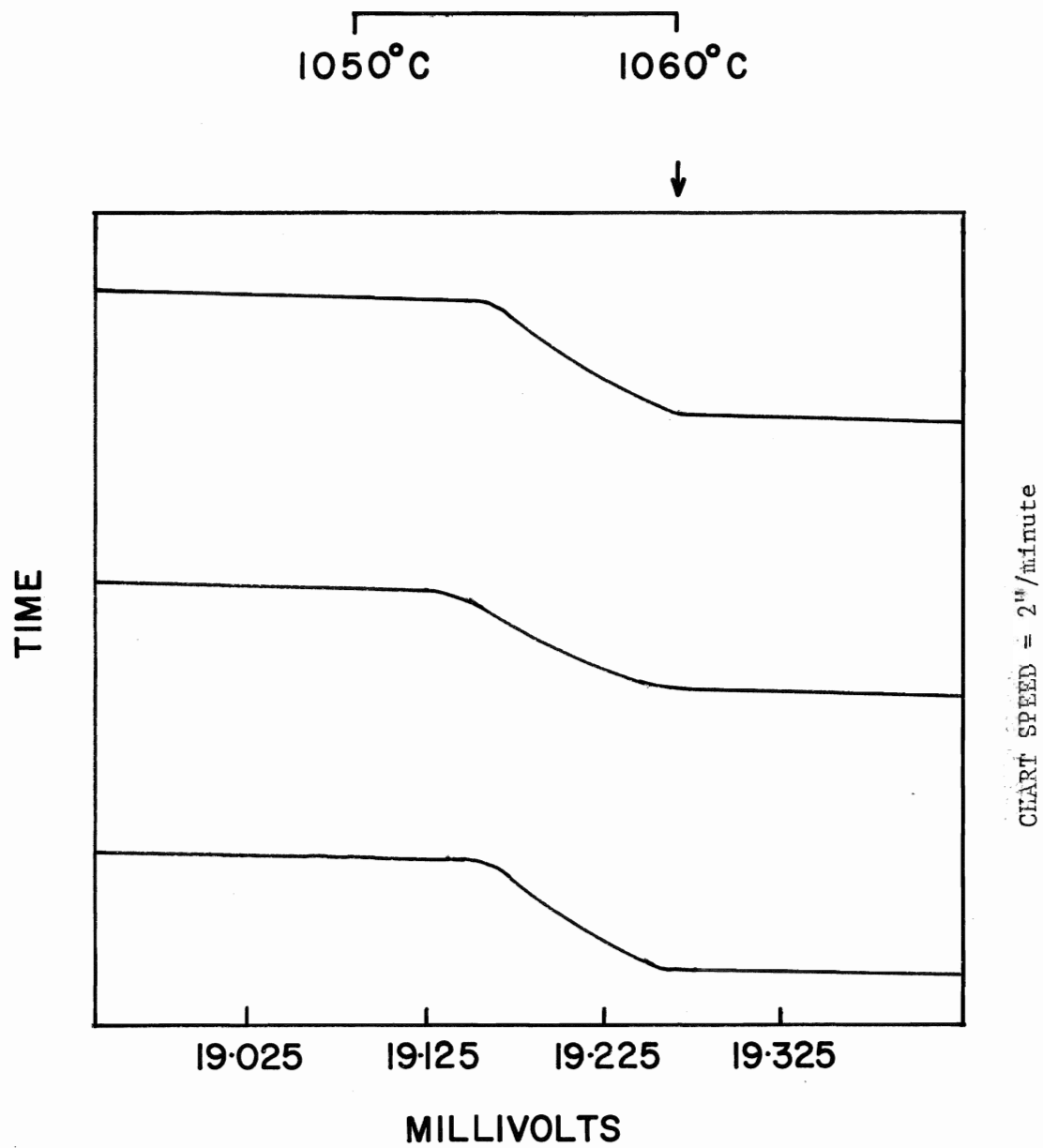


Fig.4.1. Determination of  $T_m$  of gold.

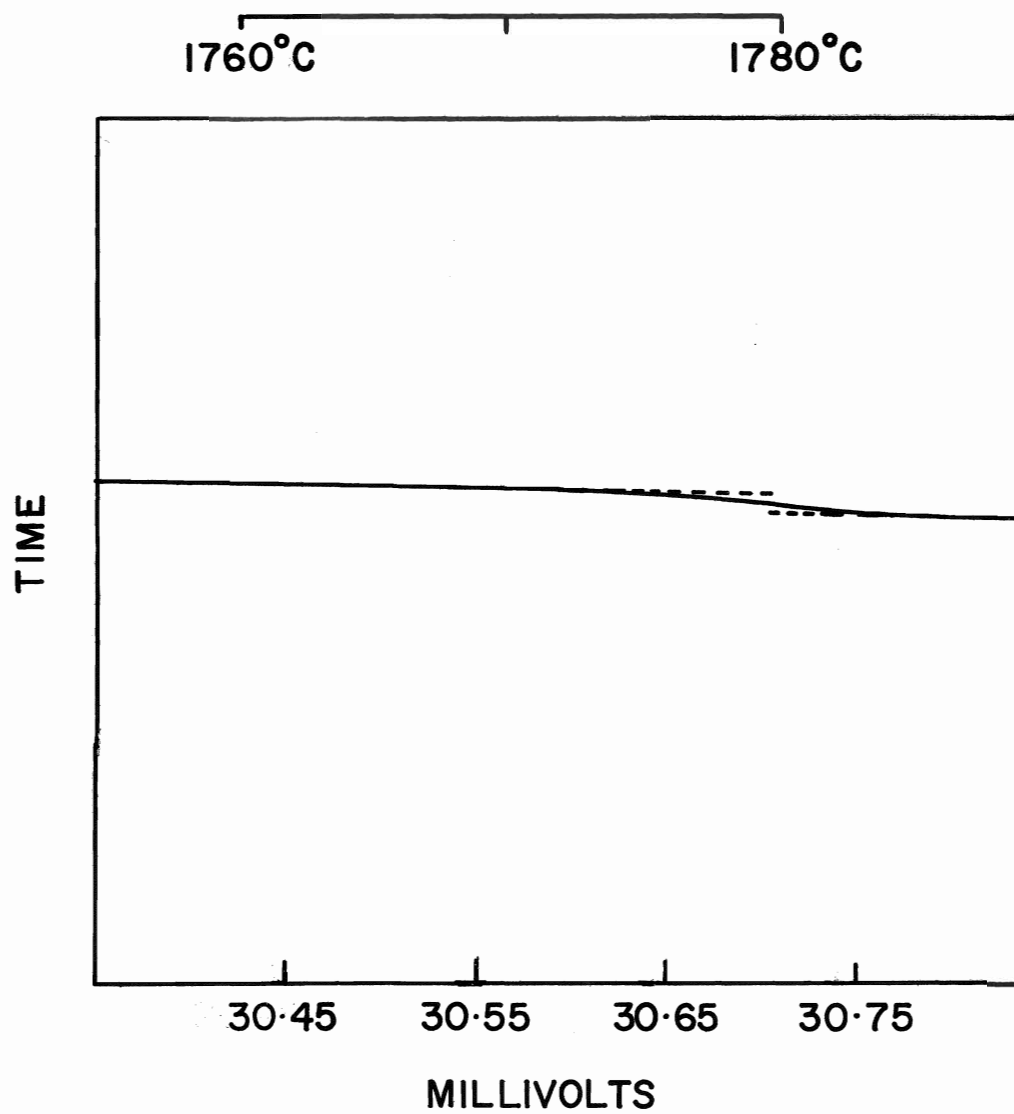


Fig.4.2.Determination of  $T_m$  of Pt.

Fig. 4.3 Diffusion of  $\text{Co}^{60}$  in  $\text{Zr}_{50}\text{Ti}_{50}$   
At  $900^{\circ}\text{C}$  for 2 hours.

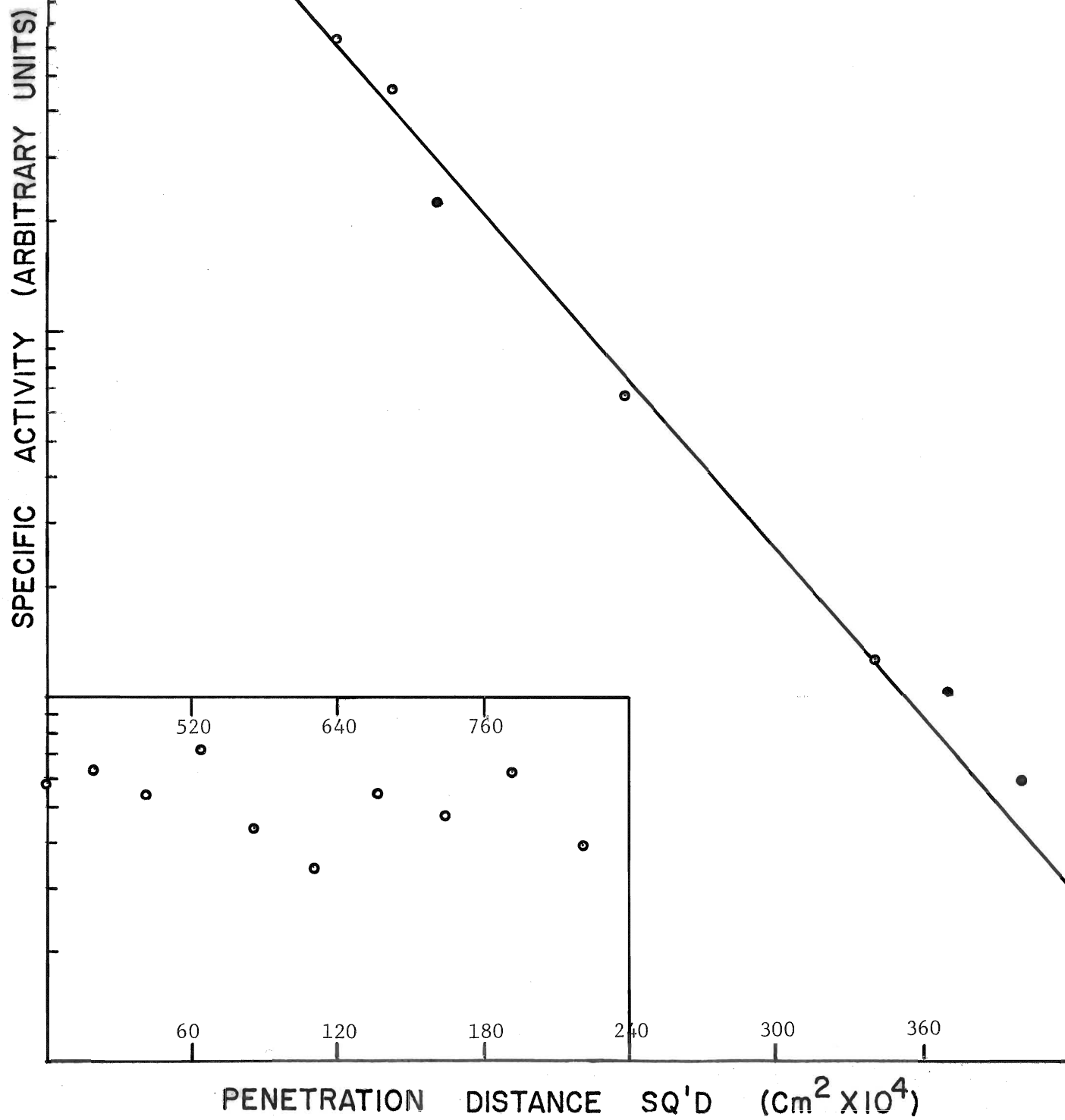


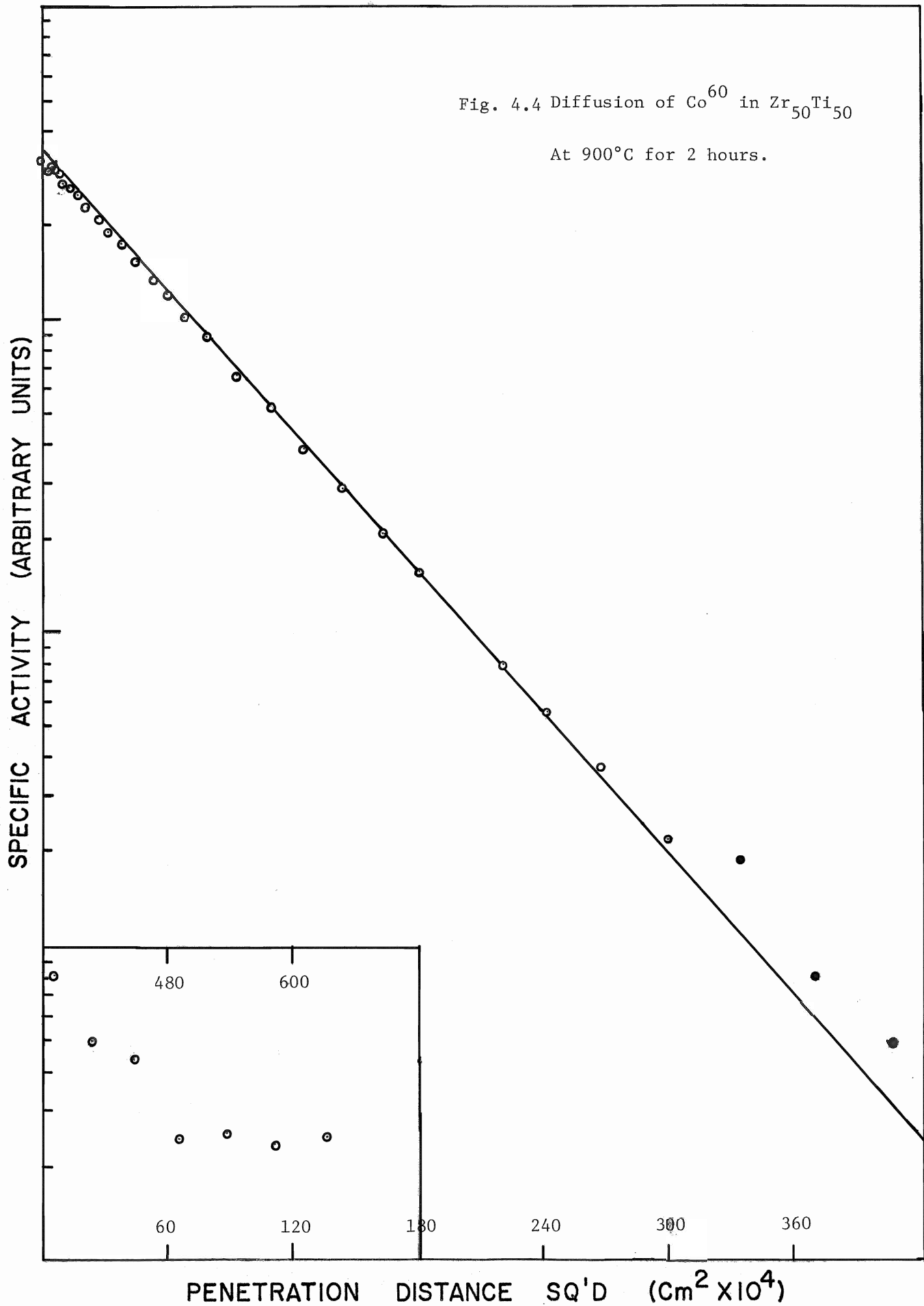
Fig. 4.4 Diffusion of  $\text{Co}^{60}$  in  $\text{Zr}_{50}\text{Ti}_{50}$ At  $900^\circ\text{C}$  for 2 hours.

Fig. 4.5 Diffusion of  $\text{Co}^{60}$  in  $\text{Zr}_{50}\text{Ti}_{50}$   
At  $1200^\circ\text{C}$  for 82 minutes.

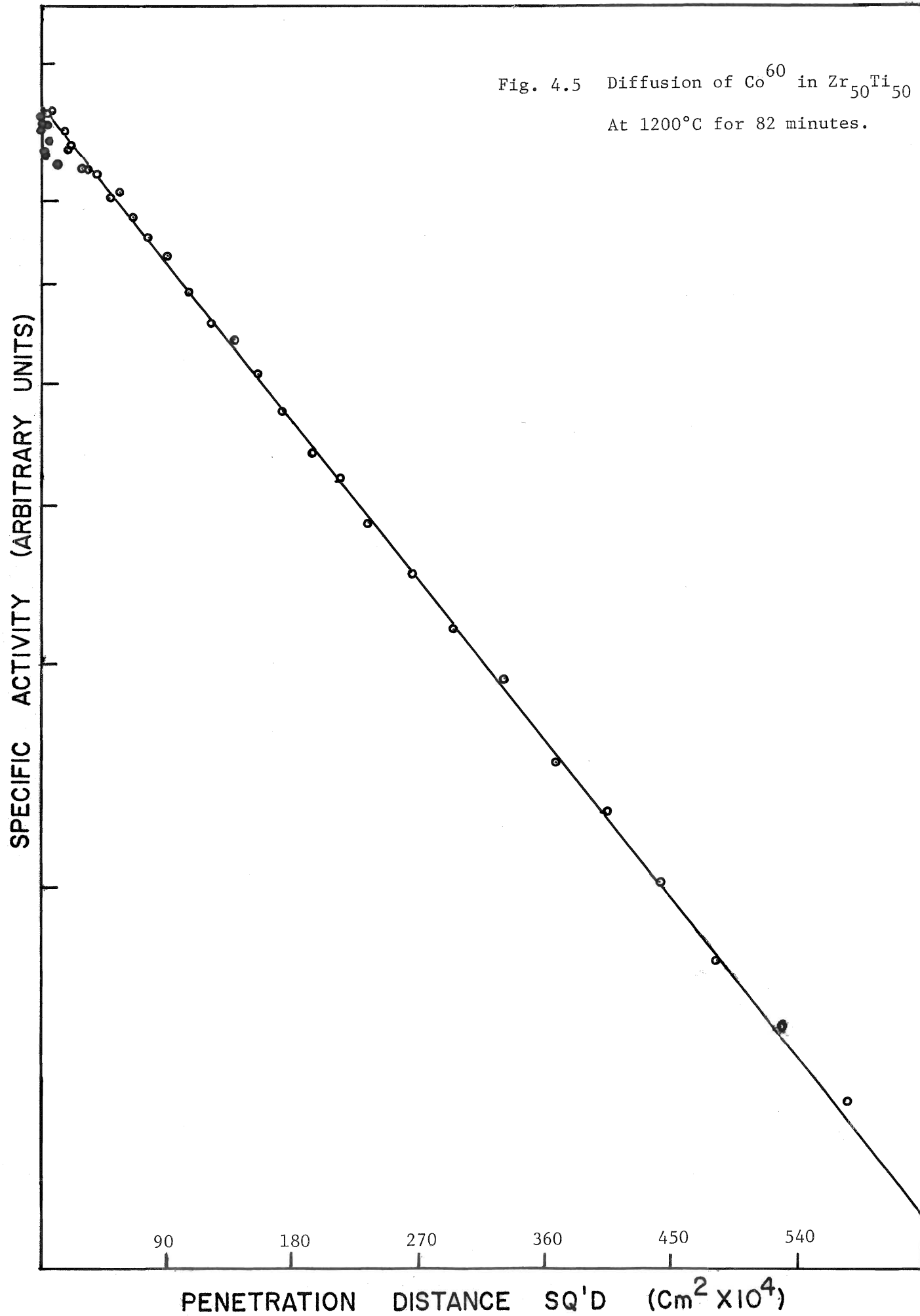


Fig. 4.6 Diffusion of  $\text{Co}^{60}$  in  $\text{Zr}_{50}\text{Ti}_{50}$   
At  $1200^{\circ}\text{C}$  for 82 minutes.

SPECIFIC ACTIVITY (ARBITRARY UNITS)

PENETRATION DISTANCE SQ'D  $(\text{Cm}^2 \times 10^4)$

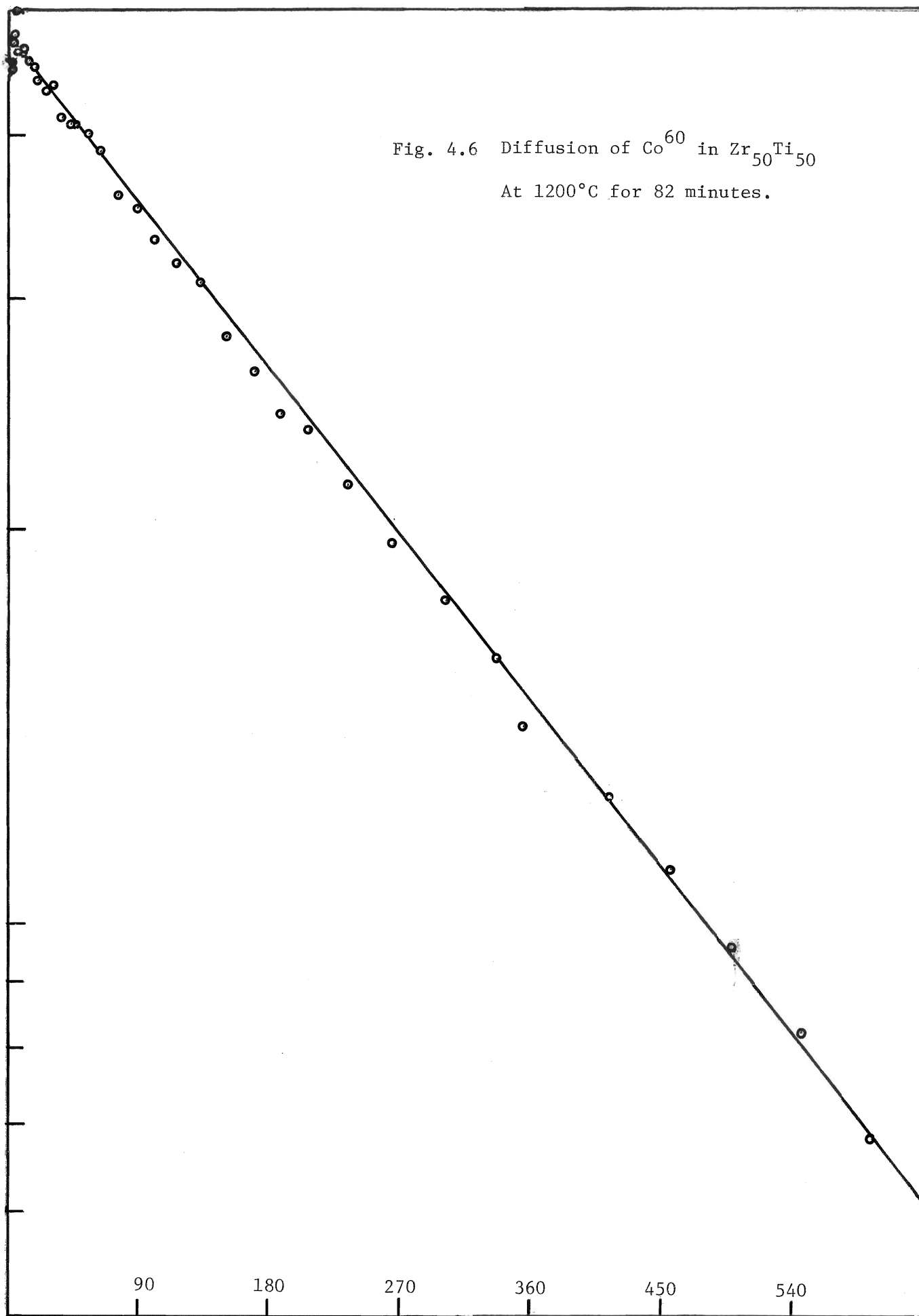
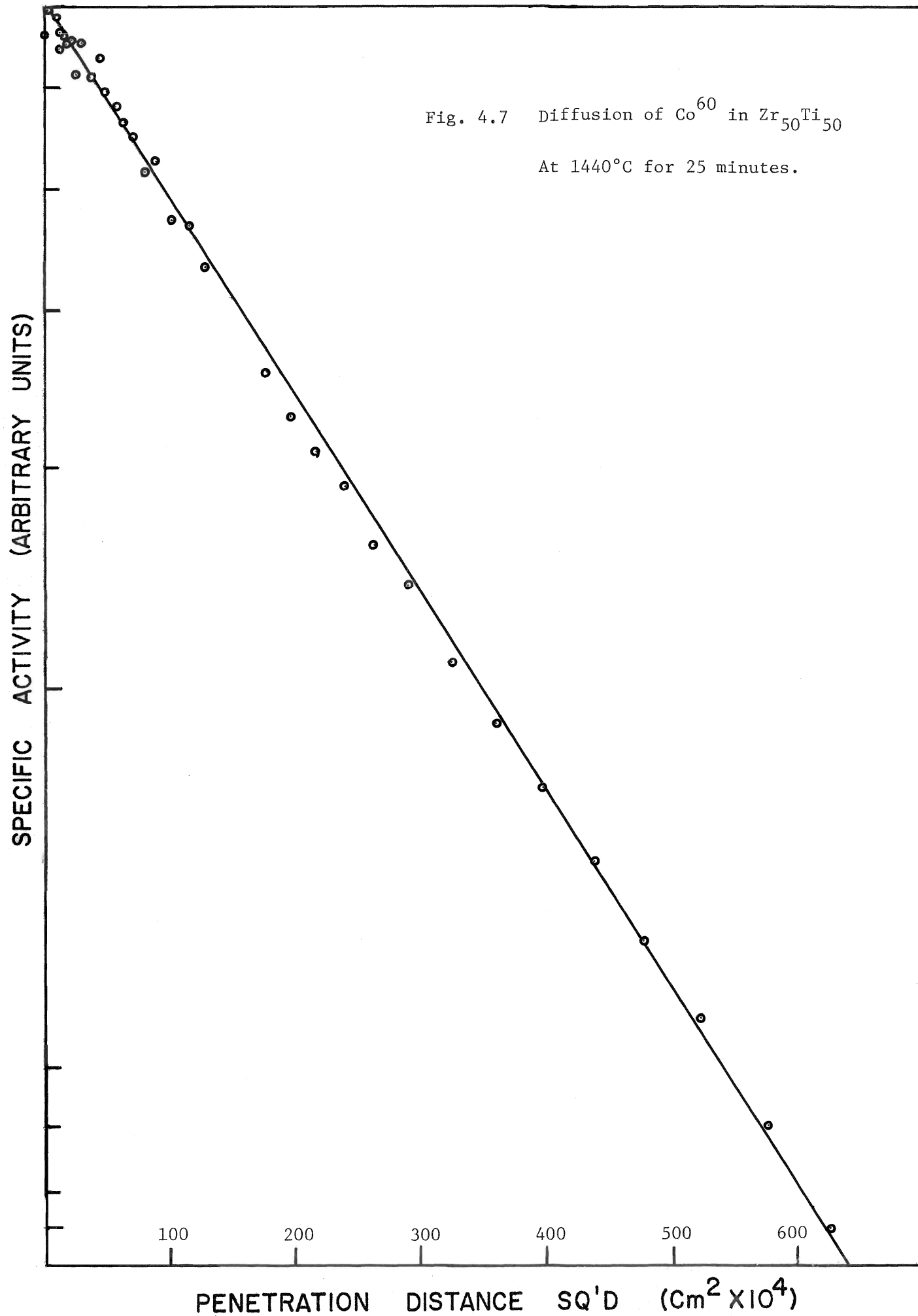


Fig. 4.7 Diffusion of  $\text{Co}^{60}$  in  $\text{Zr}_{50}\text{Ti}_{50}$

At  $1440^\circ\text{C}$  for 25 minutes.



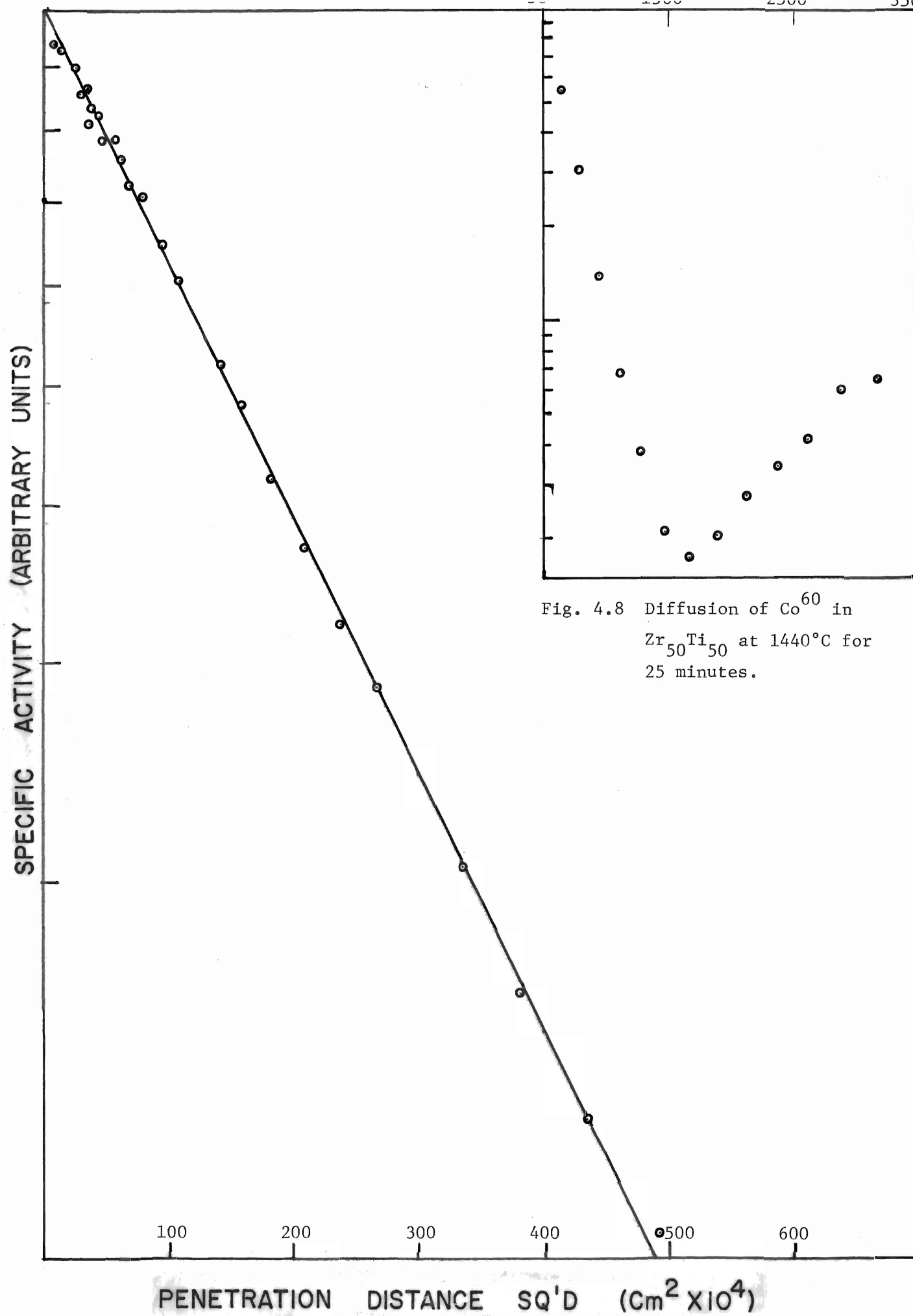
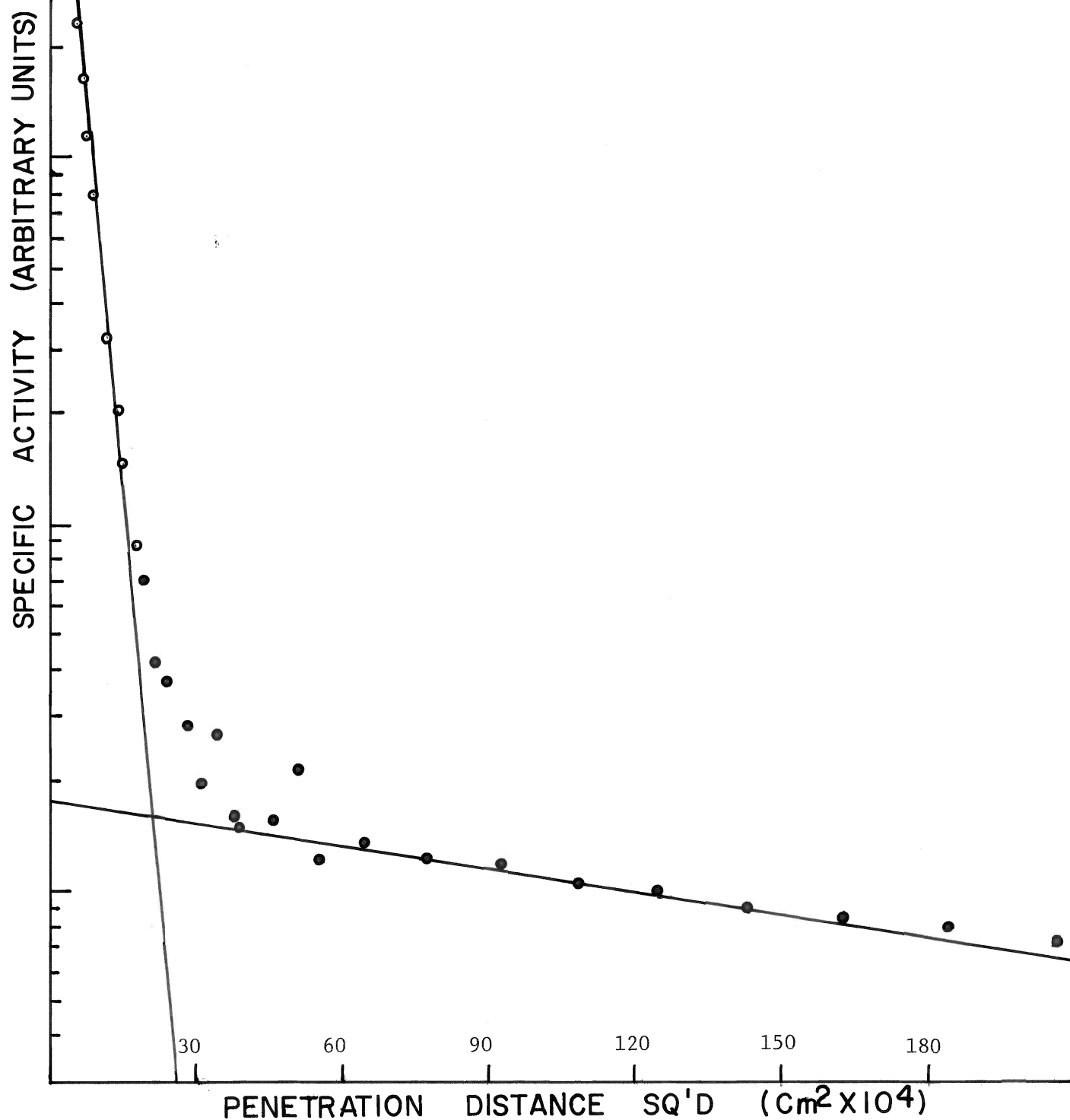




Fig. 4.9 Diffusion of  $\text{Co}^{60}$  in  $\text{Zr}_{50}\text{Ti}_{50}$   
 At  $900^\circ\text{C}$  for 2 hours. Specimen  
 pre-annealed at  $1581^\circ\text{C}$  for  $2\frac{1}{2}$   
 hours and at  $1392^\circ\text{C}$  for 2 hours,  
 before radioactive cobalt was  
 evaporated.  
 Tracer evaporated while the  
 temperature of the specimen was  
 maintained at  $900^\circ\text{C}$ .



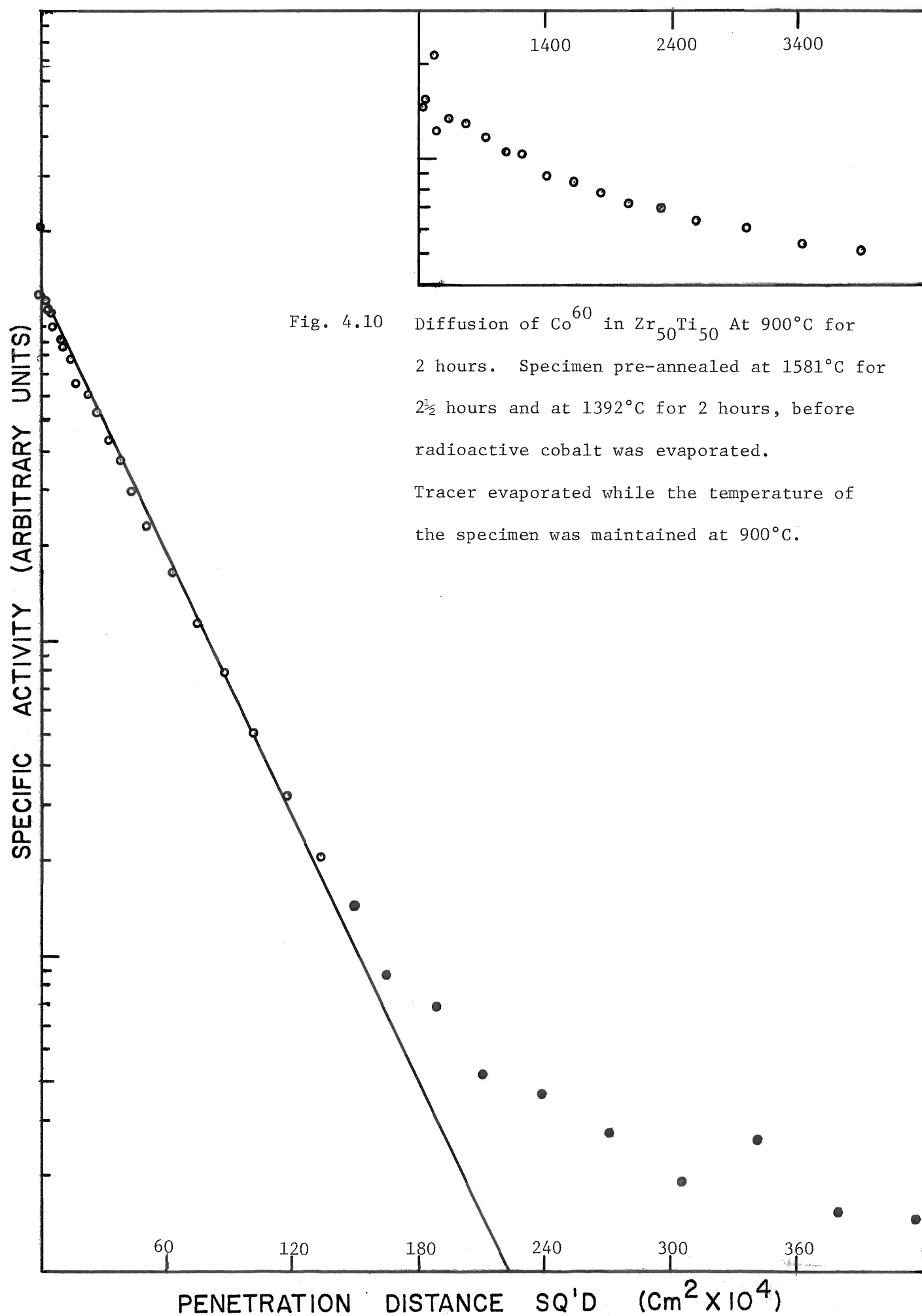


Fig. 4.10 Diffusion of  $\text{Co}^{60}$  in  $\text{Zr}_{50}\text{Ti}_{50}$  At  $900^\circ\text{C}$  for 2 hours. Specimen pre-annealed at  $1581^\circ\text{C}$  for  $2\frac{1}{2}$  hours and at  $1392^\circ\text{C}$  for 2 hours, before radioactive cobalt was evaporated. Tracer evaporated while the temperature of the specimen was maintained at  $900^\circ\text{C}$ .

Fig. 4.11 Diffusion of  $\text{Co}^{60}$  in  $\text{Zr}_{50}\text{Ti}_{50}$   
Reproducibility of Data for the  
Runs at  $900^\circ\text{C}$ .

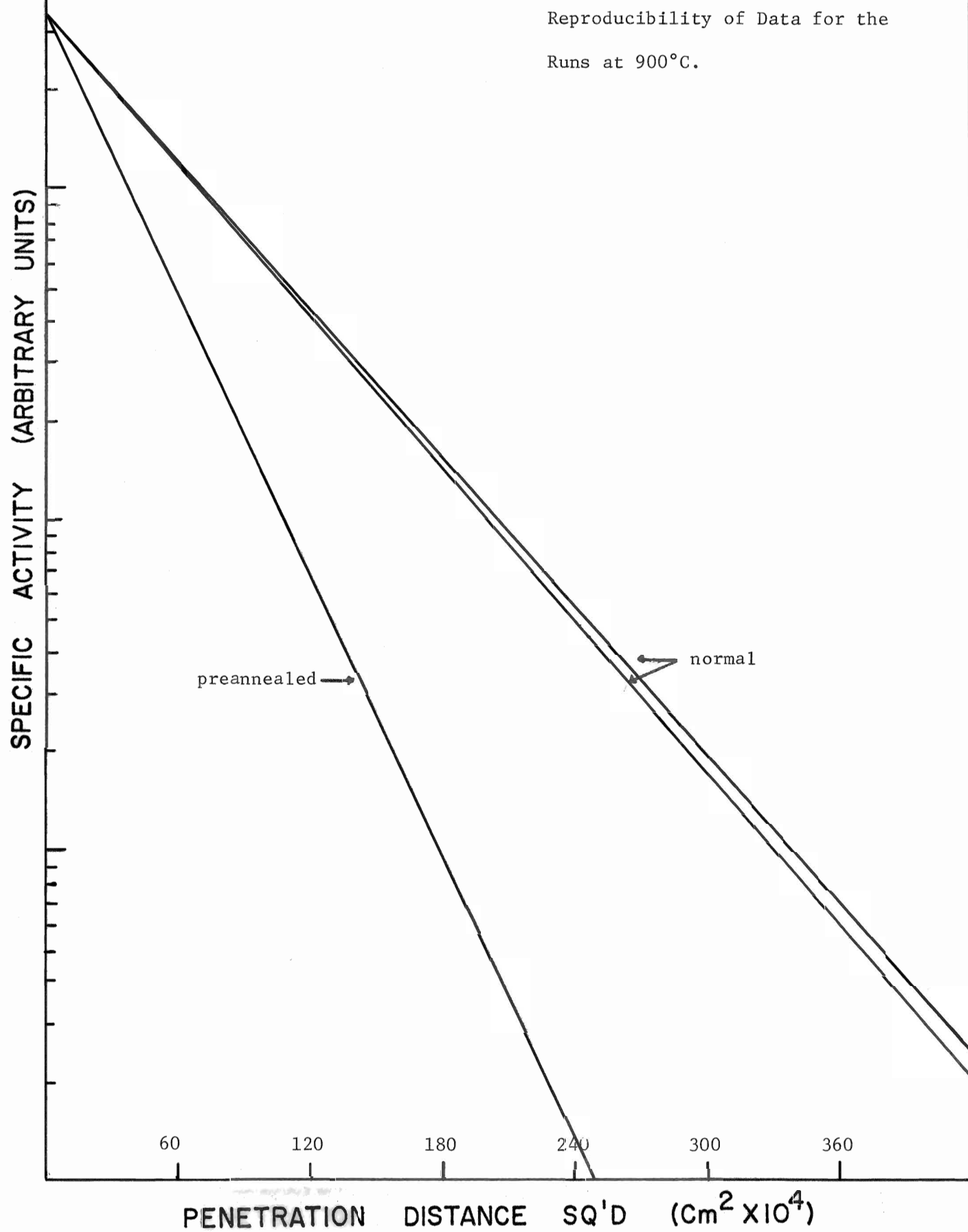


Fig. 4.12 Diffusion of  $\text{Co}^{60}$  in  $\text{Zr}_{50}\text{Ti}_{50}$   
Reproducibility of Data for the  
Runs at  $1200^\circ\text{C}$ .

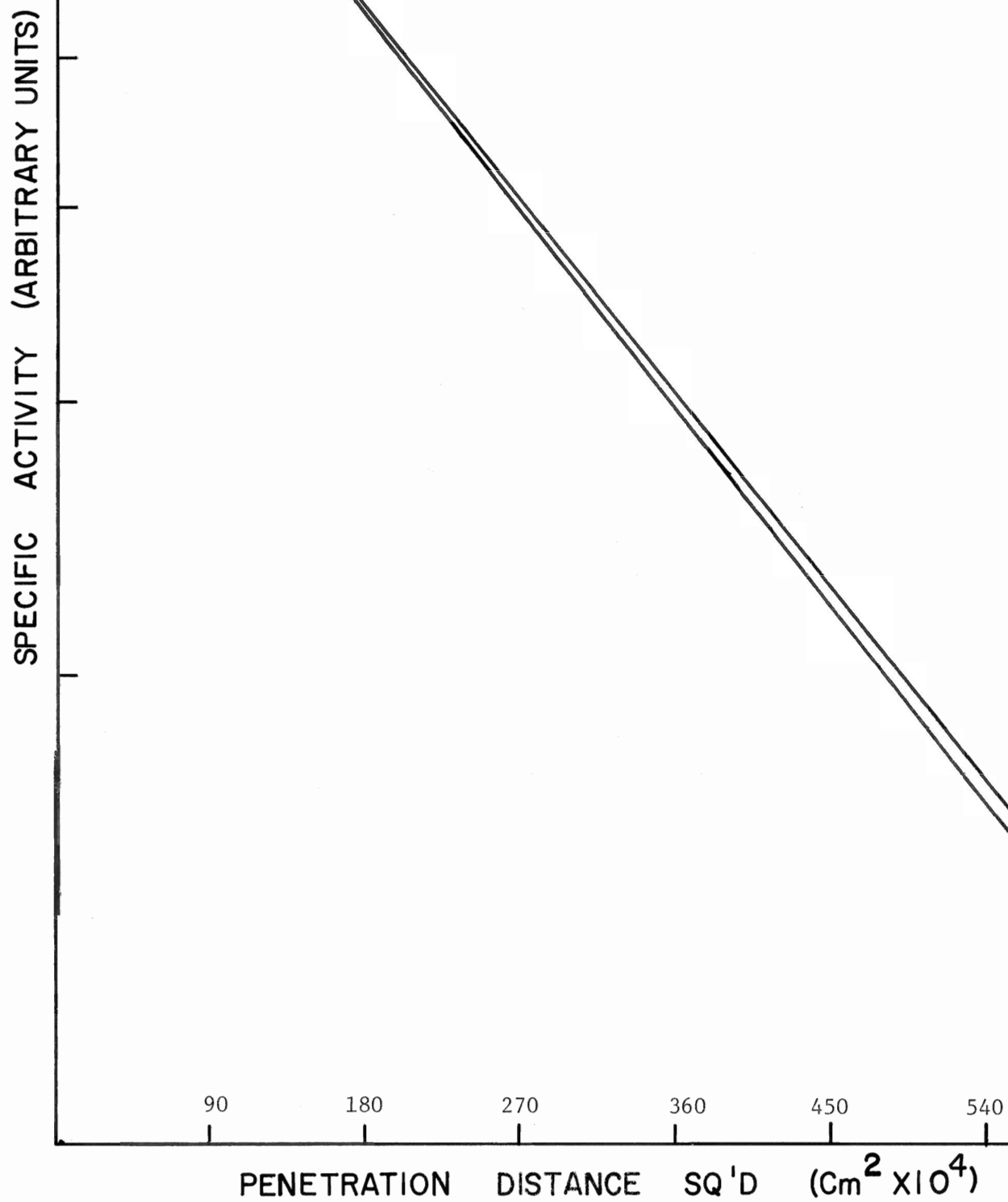


Fig. 4.13 Diffusion of  $\text{Co}^{60}$  in  $\text{Zr}_{50}\text{Ti}_{50}$   
Reproducibility of Data for  
the Runs at  $1440^\circ\text{C}$ .

SPECIFIC ACTIVITY (ARBITRARY UNITS)

100 200 300 400 500 600  
PENETRATION DISTANCE  $\text{SQ}'\text{D}$  ( $\text{Cm}^2 \times 10^4$ )

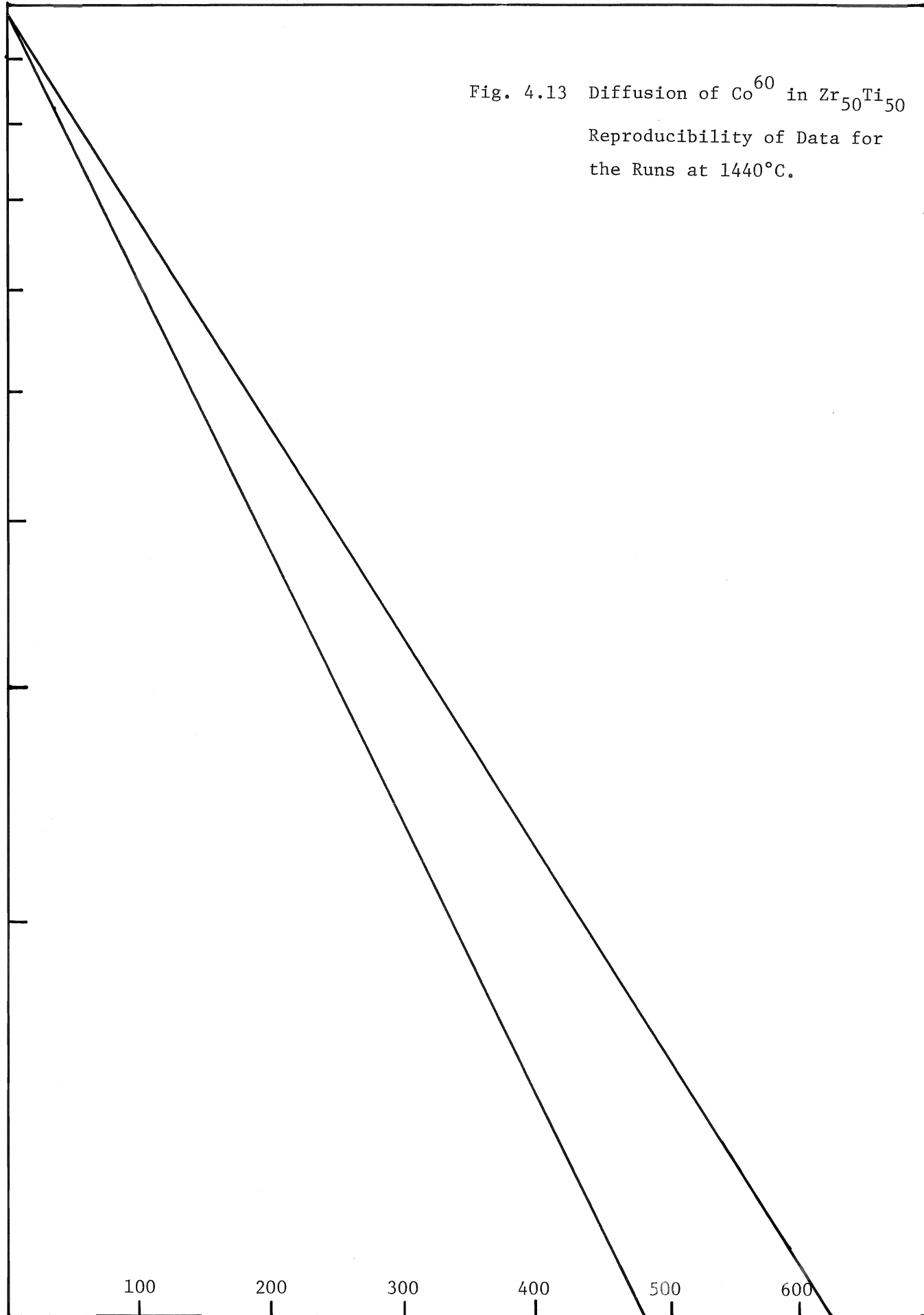
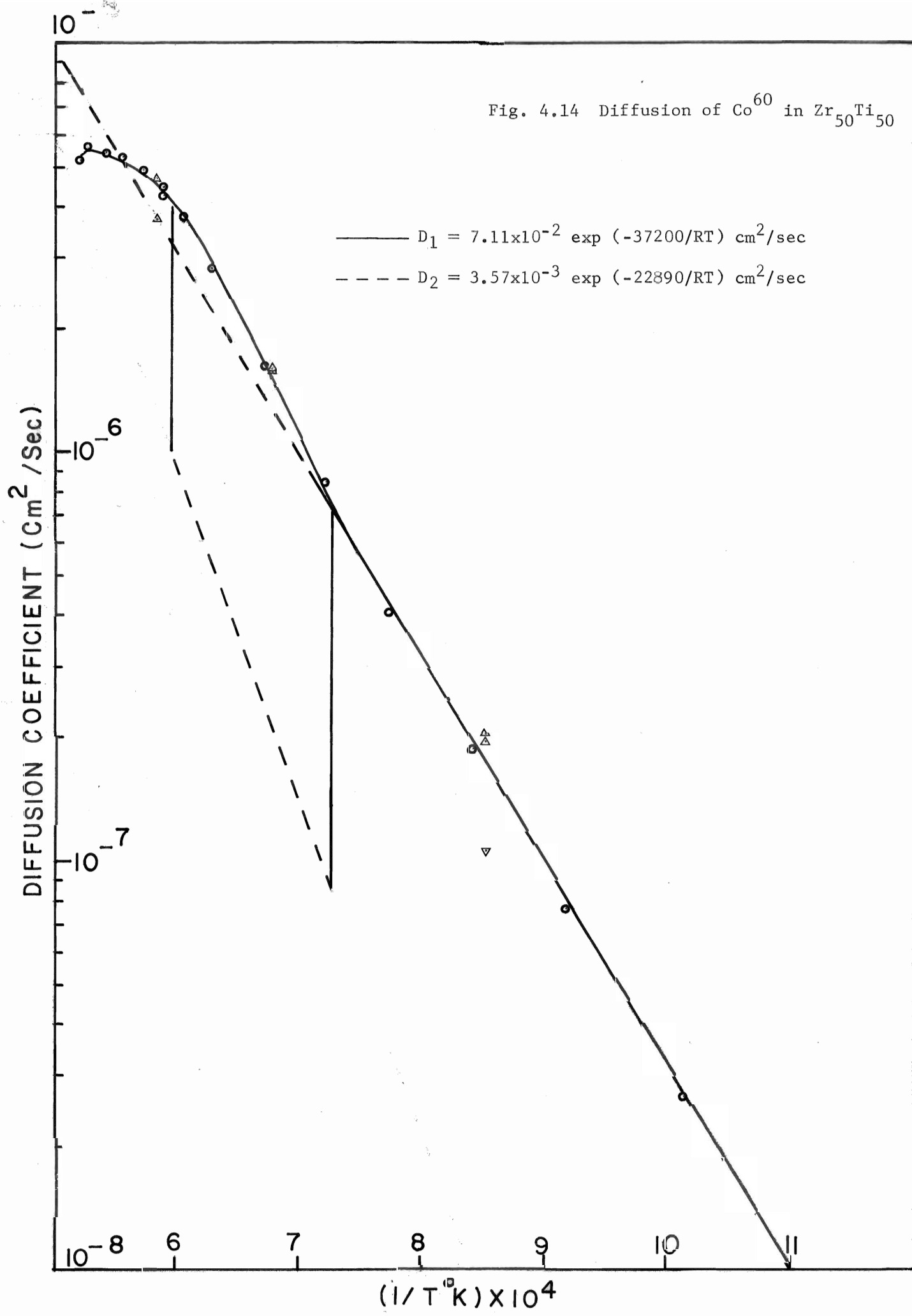


Fig. 4.14 Diffusion of  $\text{Co}^{60}$  in  $\text{Zr}_{50}\text{Ti}_{50}$ 

## CHAPTER V. DISCUSSION

The essential results of this study can be summarized as follows:

(i) The rapid diffusion of  $\text{Co}^{60}$  in the B.C.C. beta phase of the  $\text{Zr}_{50}\text{Ti}_{50}$  alloy, as initially determined by Kidson (17) has been confirmed.

(ii) As was noted for the diffusion of  $\text{Co}^{60}$  in the B.C.C. beta phase of pure zirconium (16), the Arrhenius plot of  $\log D$  versus  $1/T$  for that solute in the  $\text{Zr}_{50}\text{Ti}_{50}$  alloy is strictly linear over an extensive range of temperatures.

(iii) Above about  $1100^{\circ}\text{C}$ , the Arrhenius plot curves upward, followed by a negative curvature beyond about  $1400^{\circ}\text{C}$ .

(iv) The possibility of attributing the latter negative curvature to an error in the temperature measurements was discounted on two grounds;

(a) in the study of the diffusion of  $\text{Co}^{60}$  in  $\beta$  Zr, using the same equipment and techniques, the Arrhenius curve was linear between  $1400^{\circ}\text{C}$  and  $1600^{\circ}\text{C}$  (b) a calibration of the tungsten-rhenium thermocouple, using the melting points of 99.999% pure gold and platinum gave agreement with established values to within  $\pm 5^{\circ}\text{C}$ .

(v) The reproducibility of the results at  $900^{\circ}\text{C}$  was within 2% and at  $1200^{\circ}\text{C}$  within 4%. At  $1440^{\circ}\text{C}$ , one of the measurements agreed within 2% with the earlier unpublished work while a second run gave a diffusion coefficient 23% lower; the source of this discrepancy is not known.

(vi) Prolonged annealing of the specimen at temperatures close to the melting point of the alloy, followed by an evaporation of the radioactive tracer layer while maintaining the specimen in the B.C.C. phase, resulted in a decrease in the diffusion coefficient by a factor of approximately two at  $900^{\circ}\text{C}$ .

(vii) A deeply penetrating "tail" was observed on some of the concentration profiles.

In the following, these results are discussed in terms of the tentative interpretation outlined in Chapter I viz., that in the low temperature region the diffusion rates are dominated by migration along dislocations and that the positive curvature arises as the vacancy mechanism begins to make a significant contribution to the total diffusion.

In particular, it is assumed that the complex shape of the Arrhenius plot reflects the contribution of two or more mechanisms to the measured diffusion coefficient  $D$ . If  $D_K$  is the diffusion coefficient associated with the  $K^{\text{th}}$  mechanism and  $\lambda_K$  the fraction of the total annealing time that the atoms, on the average, spend diffusing via that mechanism, then as shown in Appendix C,

$$D = \sum_K D_K \lambda_K \quad (5.1)$$

The simplest assumption, of course, is that only two mechanisms are operative. Thus equation (5.1) can be written as

$$D = D_1(1-\lambda) + \lambda D_2 \quad (5.2)$$

While the continuous curvature in the Arrhenius plot for self diffusion in  $\beta$  Zr (10) made any resolution of  $D$  into its components ambiguous, such is not the case in the present study. Here the low temperature region is strictly linear indicating that the mechanism associated with  $D_2$  is completely dominant. Thus by subtracting the extrapolated curve from the measured  $D$  in the region  $1100^\circ - 1400^\circ\text{C}$ , one obtains the unique resolution:

$$D = 7.11 \times 10^{-2} \exp(-37200/RT) + 3.57 \times 10^{-3} \exp(-22890/RT) \text{ cm}^2/\text{sec}.$$

A comparison of the temperature dependence of  $D_1$  with that associated with



self diffusion by the single vacancy mechanism in  $\beta$  Zr (10) suggests that  $D_1$  can also be associated with this mechanism.

Let it further be assumed that  $\lambda D_2$  represents the contribution from diffusion along a dislocation network introduced during the martensitic phase transformation from the room temperature close packed hexagonal structure to the high temperature body centered cubic structure.

Following the analyses of Hart (13) and Mortlock (28),  $\lambda$  is then a product of two factors (i)  $g$ , the fraction of sites associated with dislocations and (ii) the segregation coefficient  $c_d/c_l$ . The former can be expressed as

$$g = \frac{n\rho}{d}$$

where  $n$  is the number of sites in a "cross section" of the dislocation,

$\rho$  the dislocation density and  $d$  the total site density or the number of sites per  $\text{cm}^2$ . The segregation coefficient can be expressed as (29)

$$\frac{c_d}{c_l} = A \exp(V/RT)$$

where the pre-exponential factor  $A$  arises from the configurational entropy and  $V$  is the "binding energy" of the solute atom to the dislocations.

If now, the low temperature linear portion of the Arrhenius plot is a measure of  $\lambda D_2$ , then

$$3.57 \times 10^{-3} \exp(-22890/RT) = \left[ \frac{n\rho}{d} A D_2^0 \right] \exp - [(Q_2 - V)/RT]$$

where  $D_2^0$  and  $Q_2$  are the pre-exponential factor and activation energy respectively, for diffusion along dislocations. Thus,

$$\rho = (3.57 \times 10^{-3}) \frac{d}{n A D_2^0} \text{ lines/cm}^2.$$

On the basis of this analysis, a range of values for  $\rho$  can be calculated for assumed values of the parameters  $d$ ,  $n$ ,  $A$  and  $D_2$ . Table V.1 summarizes the calculations.

It is apparent from the table, that if  $D_2$  is to be attributed entirely to diffusion along dislocations, the density  $\rho$  must be a minimum of about  $10^7$  lines/cm<sup>2</sup>, but could be as high as  $3 \times 10^{13}$  lines/cm<sup>2</sup>.

While this model has been criticised in the past on the grounds that a large dislocation density would be quickly reduced to a value of about  $10^6$  lines/cm<sup>2</sup> at the elevated diffusion temperatures, we note that such a process is consistent with the complex shape of the Arrhenius curve at the high temperatures wherein the falling of the diffusion coefficient reflects a decrease in the contribution from some non-equilibrium defect.

This interpretation is further supported by the two-fold reduction in the measured diffusion coefficient at 900°C for the specimen that was given a prolonged preanneal at elevated temperatures prior to the deposition of the tracer. A similar effect has been reported by Graham and Hanes Jr. (30) for the diffusion of Nb<sup>95</sup> in  $\beta$  Zirconium.

Nevertheless, there are aspects of the present and related studies that are difficult to reconcile with the above interpretation. One of these is the dislocation density deduced from the measurements; while  $\rho$  may be as low as  $10^7$  lines/cm<sup>2</sup>, this value requires the assumption of relatively large values for  $A$ ,  $n$  and  $D_d^0$ .

Most of the specimens after the diffusion anneal showed large grains in the beta phase. Thus the model implies that large dislocation densities persist during extensive grain growth.

A third aspect concerns observations of rapid diffusion of certain

transition metal solutes in well annealed single crystals of pure zirconium as reported by Hood and Schultz (14). These authors have suggested that Fe, Ni and Co diffuse at least partially via an interstitial mechanism in both the close packed hexagonal and the body centered cubic structures of zirconium.

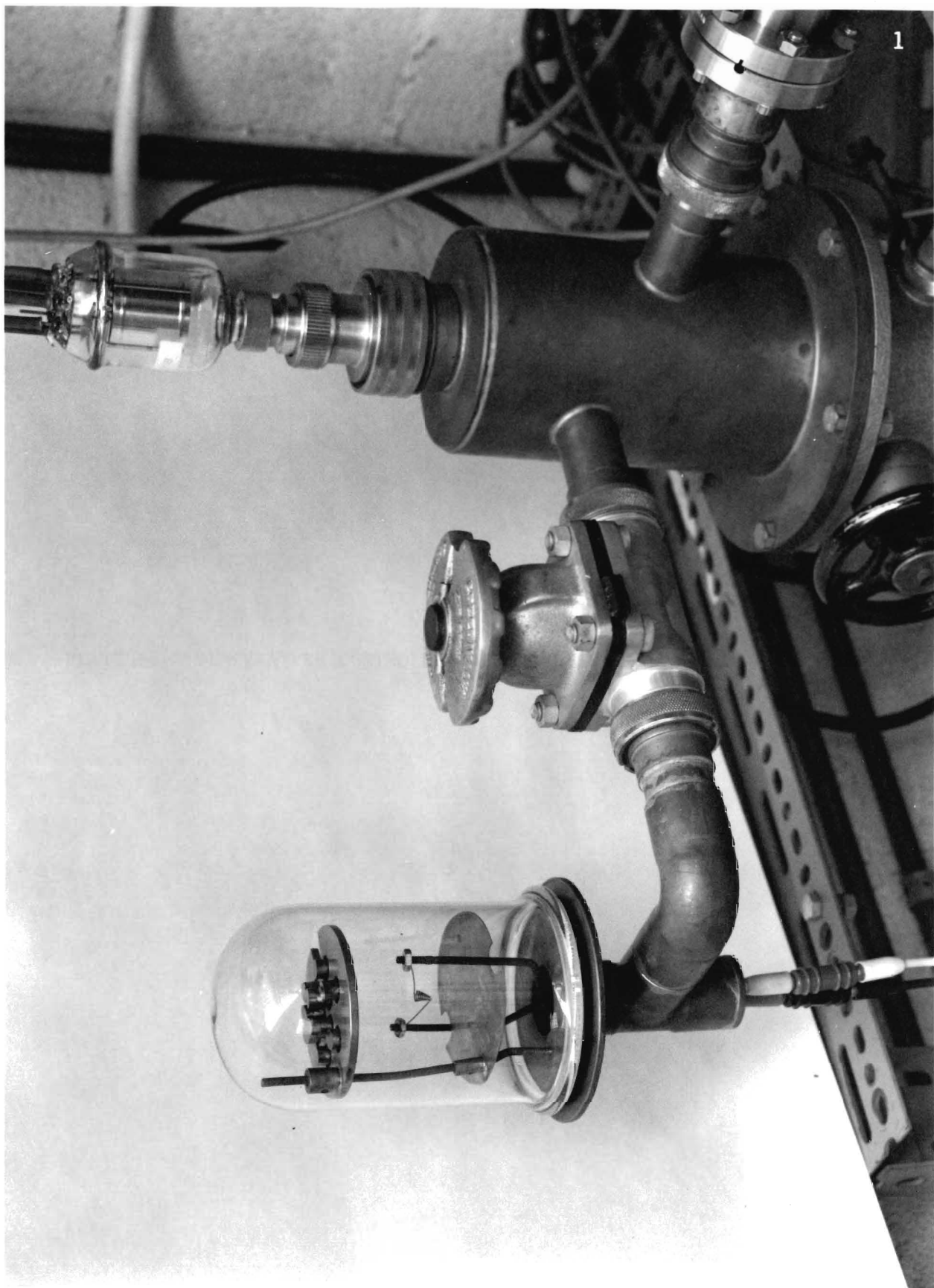
d	n	$D_d^o$	A	$\rho$
$10^{15}$	10	$10^{-2}$	1	$3.57 \times 10^{13}$
			10	$3.57 \times 10^{12}$
			25	$1.43 \times 10^{12}$
			50	$7.14 \times 10^{11}$
$10^{15}$	10	$10^{-1}$	1	$3.57 \times 10^{12}$
			10	$3.57 \times 10^{11}$
			25	$1.43 \times 10^{11}$
			50	$7.14 \times 10^{10}$
$10^{15}$	10	1	1	$3.57 \times 10^{11}$
			10	$3.57 \times 10^{10}$
			25	$1.43 \times 10^{10}$
			50	$7.14 \times 10^9$
$10^{15}$	10	10	1	$3.57 \times 10^{10}$
			10	$3.57 \times 10^9$
			25	$1.43 \times 10^9$
			50	$7.14 \times 10^8$
$10^{15}$	10	100	1	$3.57 \times 10^9$
			10	$3.57 \times 10^8$
			25	$1.43 \times 10^8$
			50	$7.14 \times 10^7$

TABLE V.1. Calculation of Dislocation Density

## CONCLUSIONS

The curved Arrhenius plot for the diffusion of  $\text{Co}^{60}$  in  $\text{Zr}_{50}\text{Ti}_{50}$  alloy was resolved into its components. A comparison of the high temperature diffusion parameters with those of the diffusion of  $\text{Co}^{60}$  in beta zirconium seems to suggest that vacancy mechanism is operative in that region. Several models have been proposed for the low temperature mechanism. A prolonged anneal in the high B.C.C. region had the effect of reducing the diffusion coefficient suggesting the possibility of the contribution of non-equilibrium defects (introduced during the phase change) to the total diffusion. Dislocations introduced during the phase change may be responsible for rapid atomic transport.

Since the mechanisms cannot be unambiguously specified, the possibility of the interstitial mechanism being operative cannot be ruled out.



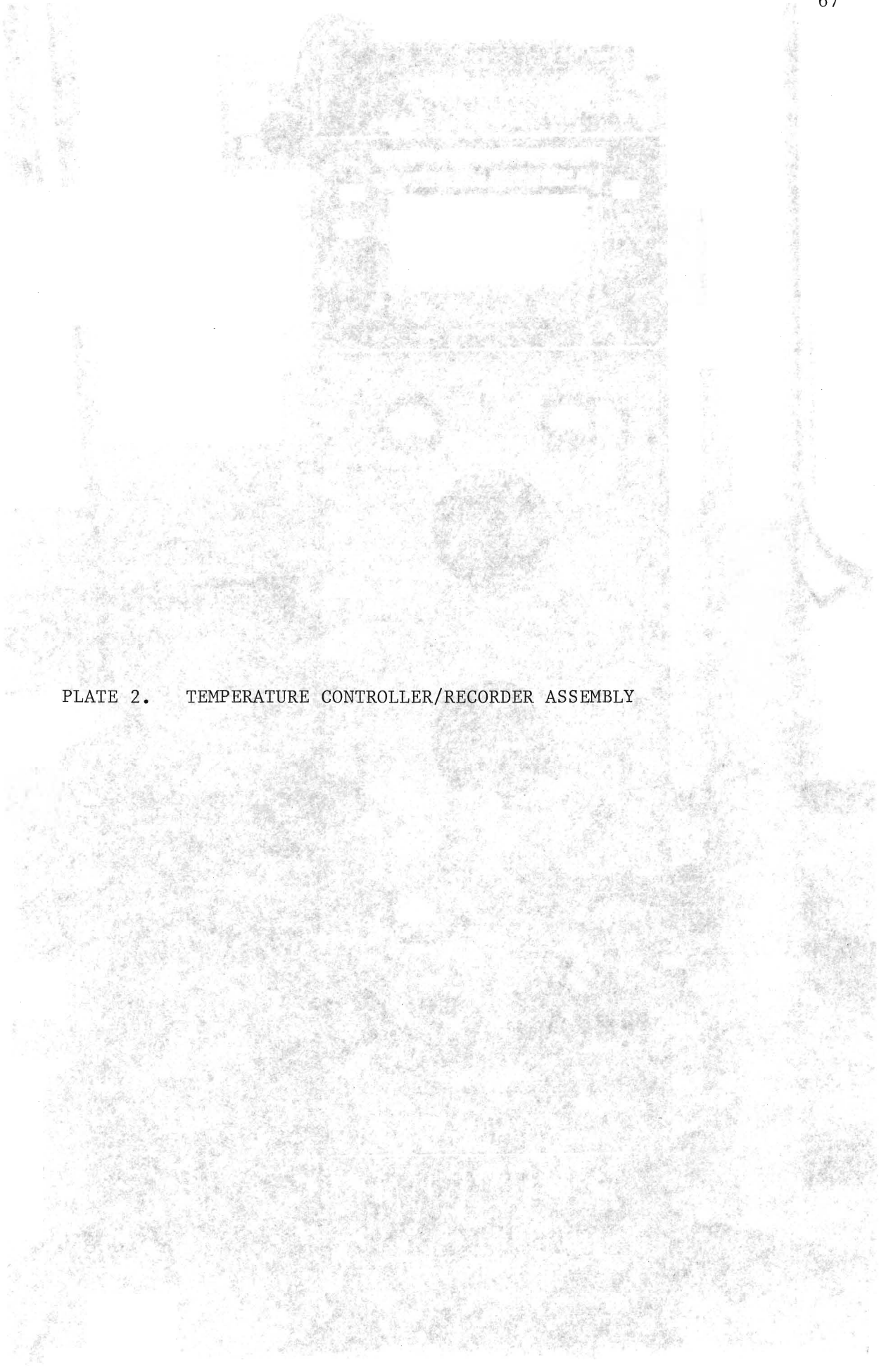
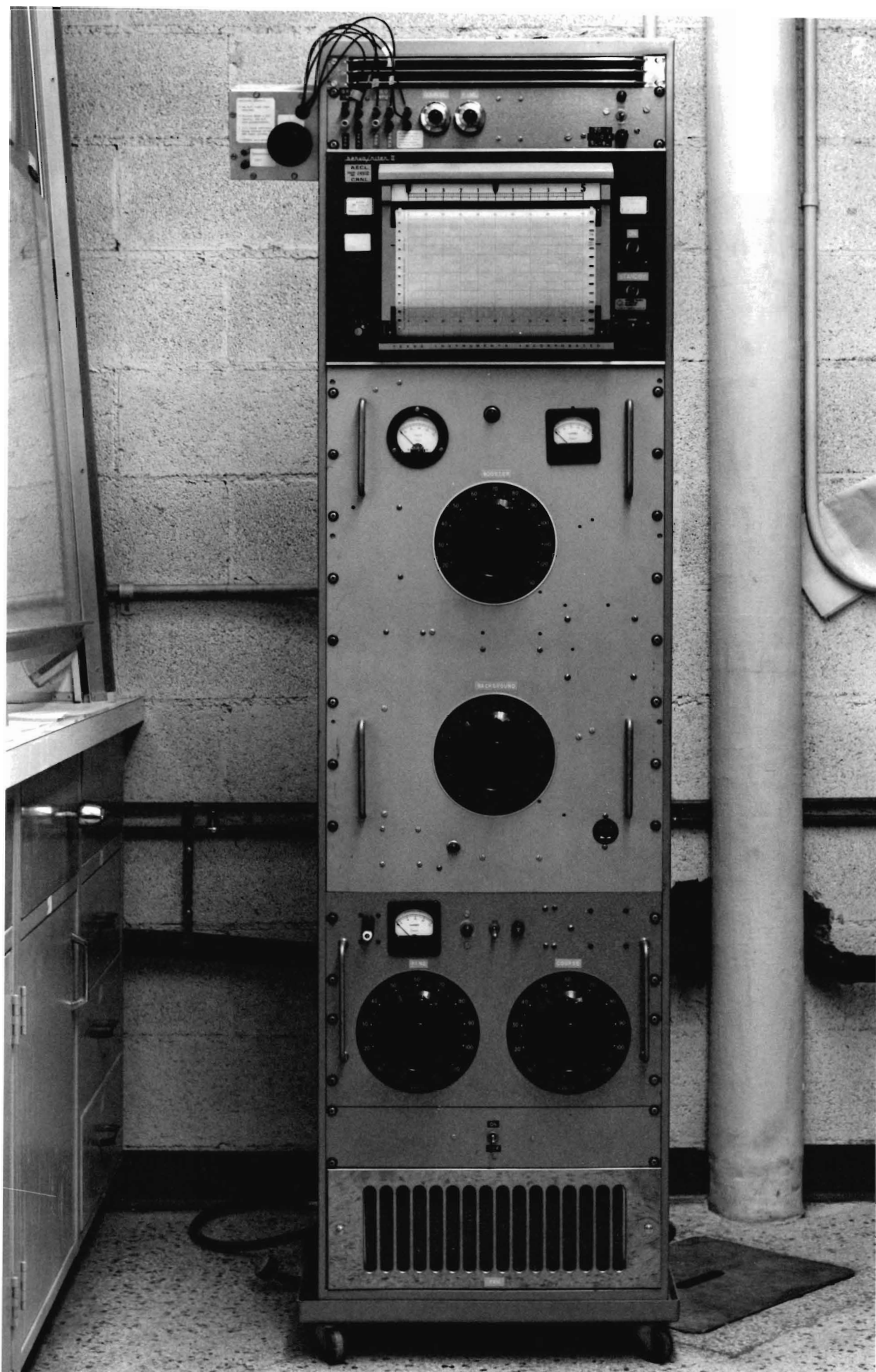


PLATE 2. TEMPERATURE CONTROLLER/RECORDER ASSEMBLY





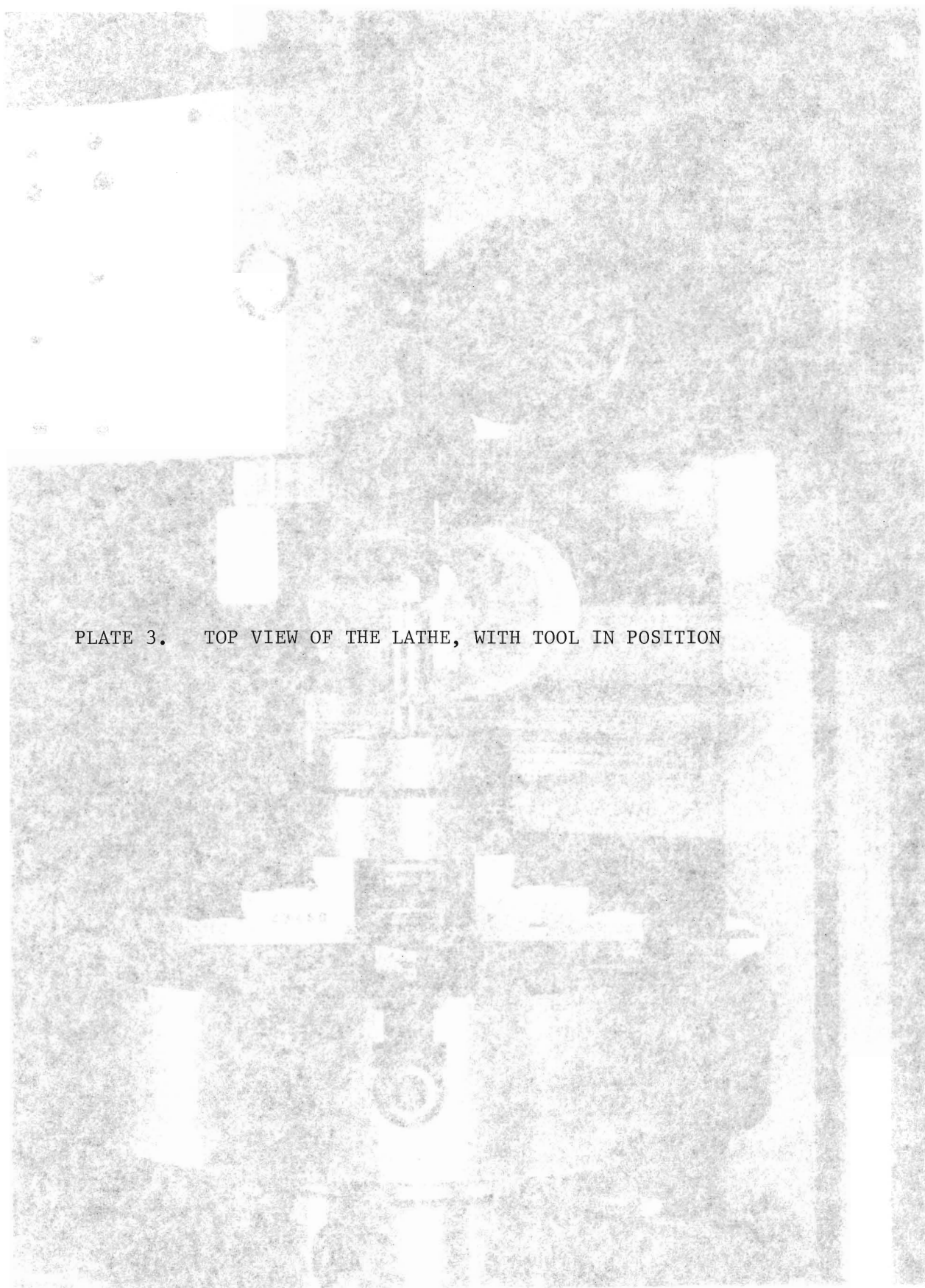


PLATE 3. TOP VIEW OF THE LATHE, WITH TOOL IN POSITION

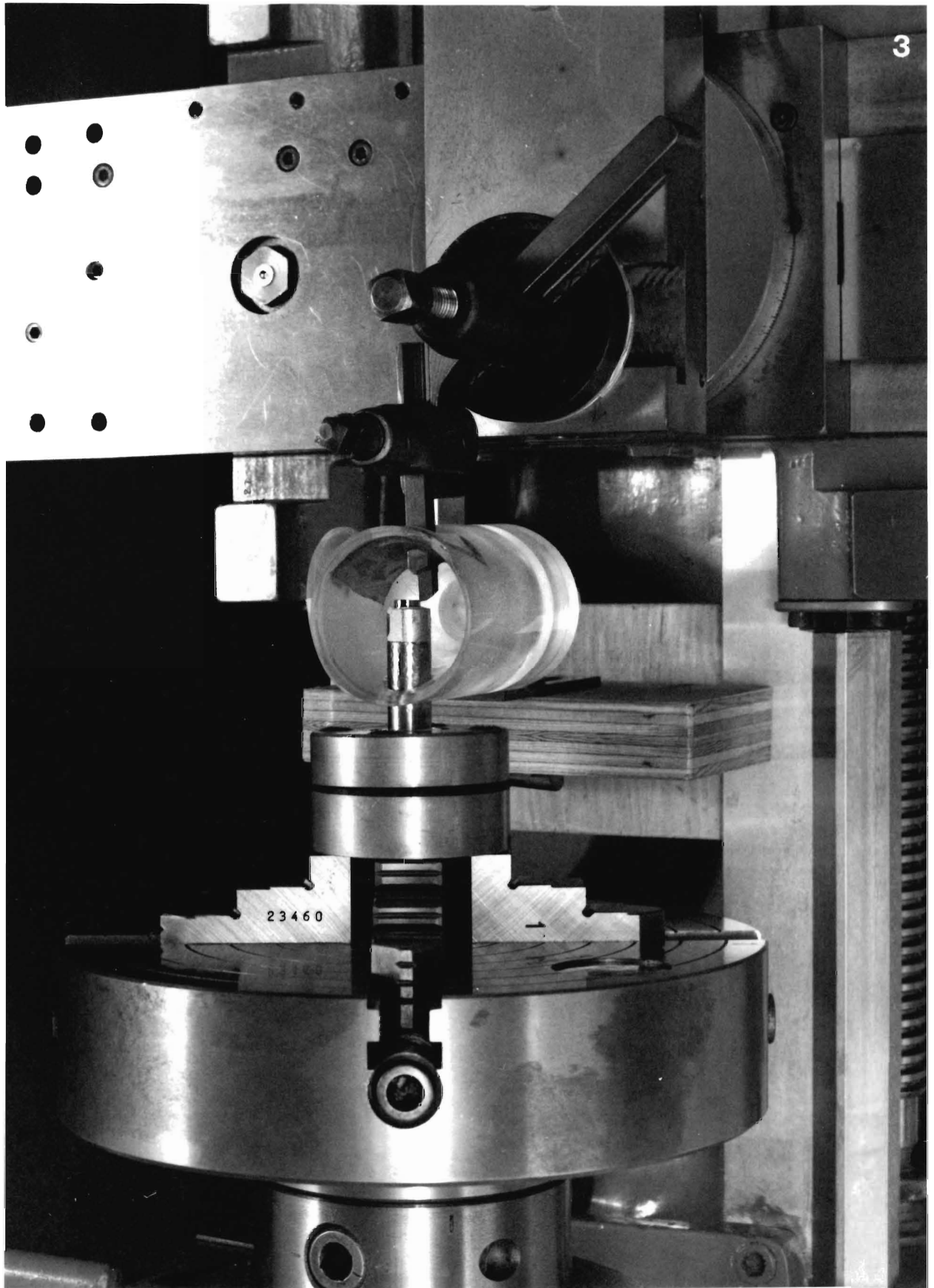


PLATE 4. COLLECTING FUNNEL SURROUNDING THE SPECIMEN



PLATE 5. DETECTION AND SCALING DEVICES

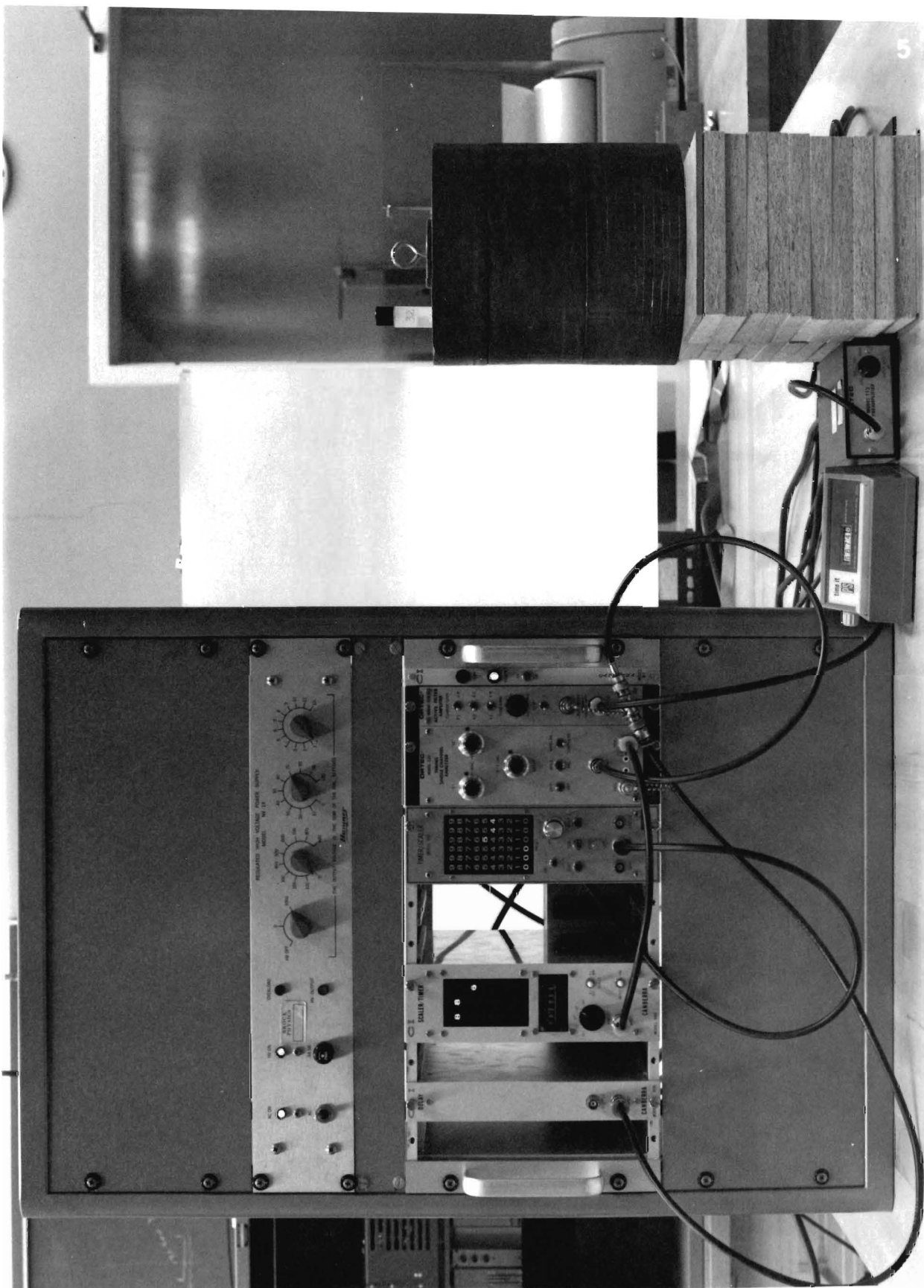


PLATE 6.    DIFFUSION FURNACE



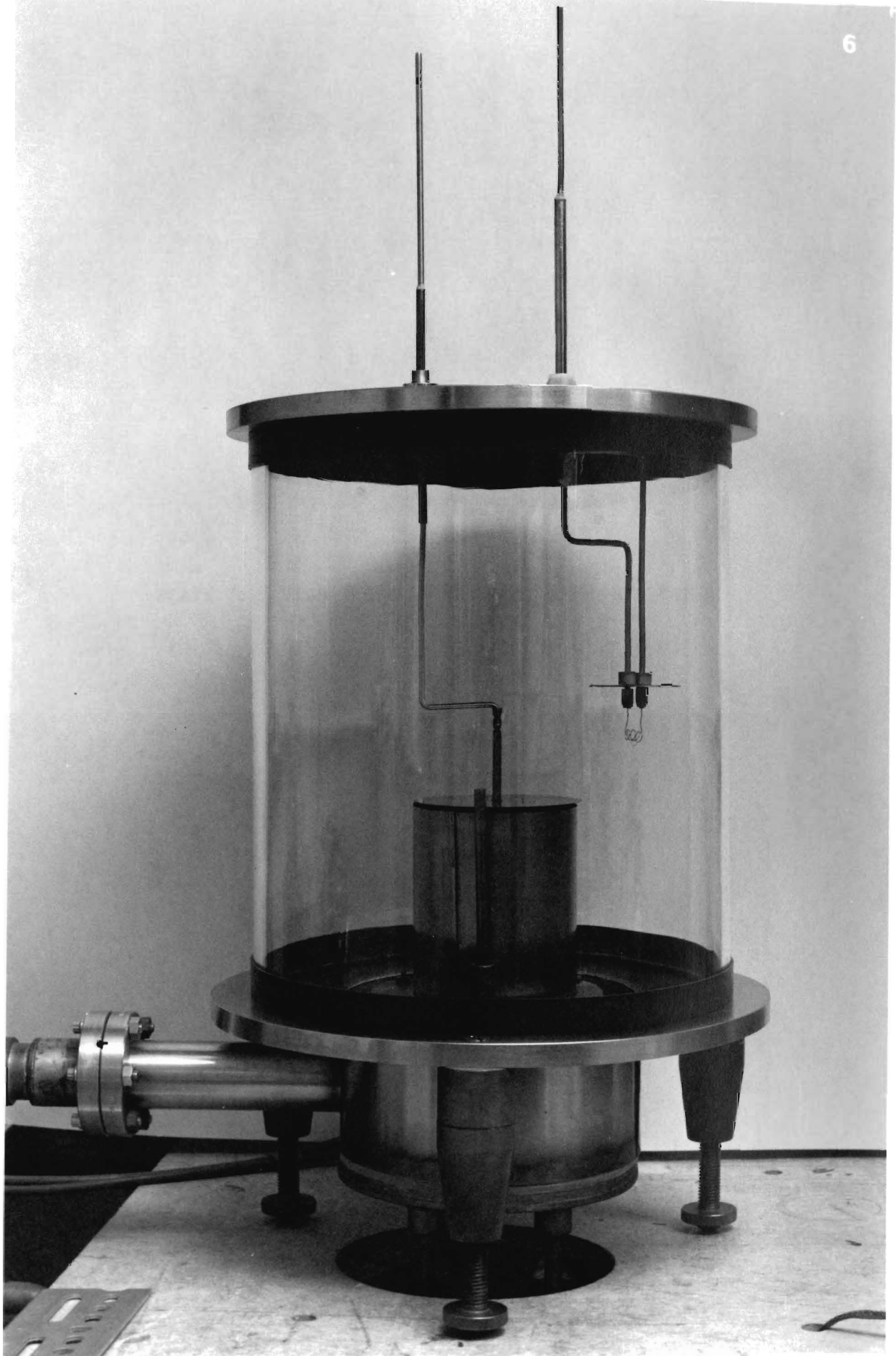
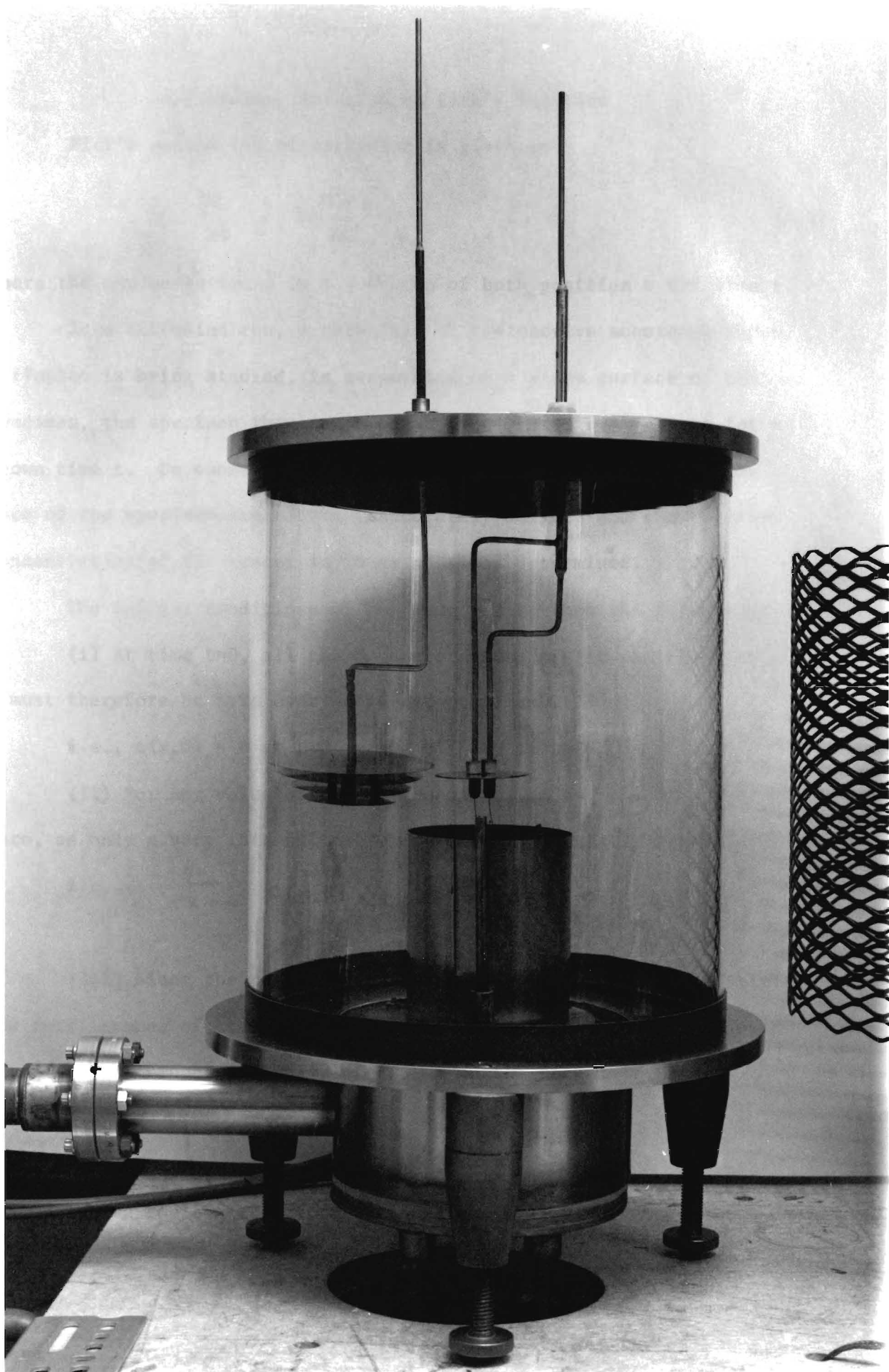




PLATE 7. HIGH TEMPERATURE EVAPORATION APPARATUS



## APPENDIX A. Solution to Fick's Equation

Fick's second law of diffusion is given as

$$\frac{\partial c}{\partial t} = D \frac{\partial^2 c}{\partial x^2} \quad (\text{A.1})$$

where the concentration  $c$  is a function of both position  $x$  and time  $t$ .

In a diffusion run, a thin film of radioactive substance whose diffusion is being studied, is evaporated on a plane surface of the specimen, the specimen then annealed at an elevated temperature for a known time  $t$ . On subsequent cooling, thin sections parallel to the face of the specimen are removed, accurately weighed and the relative concentration of the tracer in these sections determined.

The initial conditions of the problem are then the following:

(i) At time  $t=0$ , all the  $S_0$  tracer atoms are at the plane  $x=0$ ;  $c$  must therefore be zero everywhere except at  $x=0$ .

i.e.,  $c(x,0) = 0$  at  $t=0$

(ii) For any value of  $t$ , the concentration as  $x \rightarrow \infty$  must be zero, as only a very thin film of the tracer is initially deposited.

i.e.,  $\lim_{x \rightarrow \infty} c(x,t) = 0$ , for  $0 \leq t < \infty$

(iii) Since the region of diffusion is between zero and infinity, the total number of tracer atoms in this region for any time  $t$  should equal  $S_0$ , the amount initially deposited on the face  $x=0$ .

i.e.,  $\int_0^{\infty} c(x,t) dx = S_0$ , for  $0 \leq t < \infty$

Taking Laplace transform of equation (A.1) with respect to time,

$$[s u(x,s) - c(x,0)] = D u_{xx}(x,s) \quad (\text{A.2})$$

where

$$u(x,s) = L \{c(x,t)\}$$

and 
$$u_{xx}(x, s) = (\partial^2 u / \partial x^2)$$

Using condition (i), equation (A.2) reduces to

The solution of this differential equation is

$$u = c_1 \exp\left(\sqrt{\frac{s}{D}} x\right) + c_2 \exp\left(-\sqrt{\frac{s}{D}} x\right) \quad (\text{A.3})$$

where  $c_1$  and  $c_2$  are the constants of integration. Taking Laplace transform of condition (ii), it can be shown that  $c_1 = 0$ .

Equation (A.3) therefore takes the form

$$u = c_2 \exp\left(-\sqrt{\frac{s}{D}} x\right)$$

The value of the constant  $c_2$  can be easily determined from the Laplace transform of condition (iii) as

$$c_2 = S_0 / \sqrt{sD}$$

Thus, the solution of the equation (A.2) becomes

$$u(x, s) = \frac{S_0}{\sqrt{sD}} \exp\left(-\sqrt{\frac{s}{D}} x\right)$$

The Inverse Laplace transform on both sides yields

$$C(x, t) = \frac{S_0}{\sqrt{\pi D t}} \exp\left(-x^2 / 4 D t\right)$$

which is the desired solution.

## APPENDIX B. Measurement of Tracer Concentration

In the following, the electronics and the procedure used for discriminating the two  $\text{Co}^{60}$  photopeaks from the full cobalt spectrum and the subsequent counting are described in detail.

A block diagram of the electronics used is illustrated in figure B.1 and the actual arrangement of the electronics shown in Plate V.

As each gamma ray strikes the scintillation phosphor, a flash of light or scintillation is produced. This is collected by the photocathode of the photomultiplier tube which produces a large number of secondary electrons.

The output of the photomultiplier is usually weak, and therefore, it is necessary to pre-condition the same so that it can be utilized in a linear amplifier system.

The output of the pre-amplifier is amplified by a linear amplifier, which produces output pulses ranging from 0 to 10 Volts.

The amplified detector response will usually exhibit all the possible interactions of the gamma ray with the crystal i.e., photoelectric and Compton scatterings, back-scattering etc. A single channel analyser is used to discriminate the two  $\text{Co}^{60}$  photopeaks of energy 1.17 and 1.33 Mev, from the rest of the spectrum.

### Calibration of the Single Channel Analyser

Figure B.2 is a block diagram of the electronics used for the calibration of the single channel analyser.

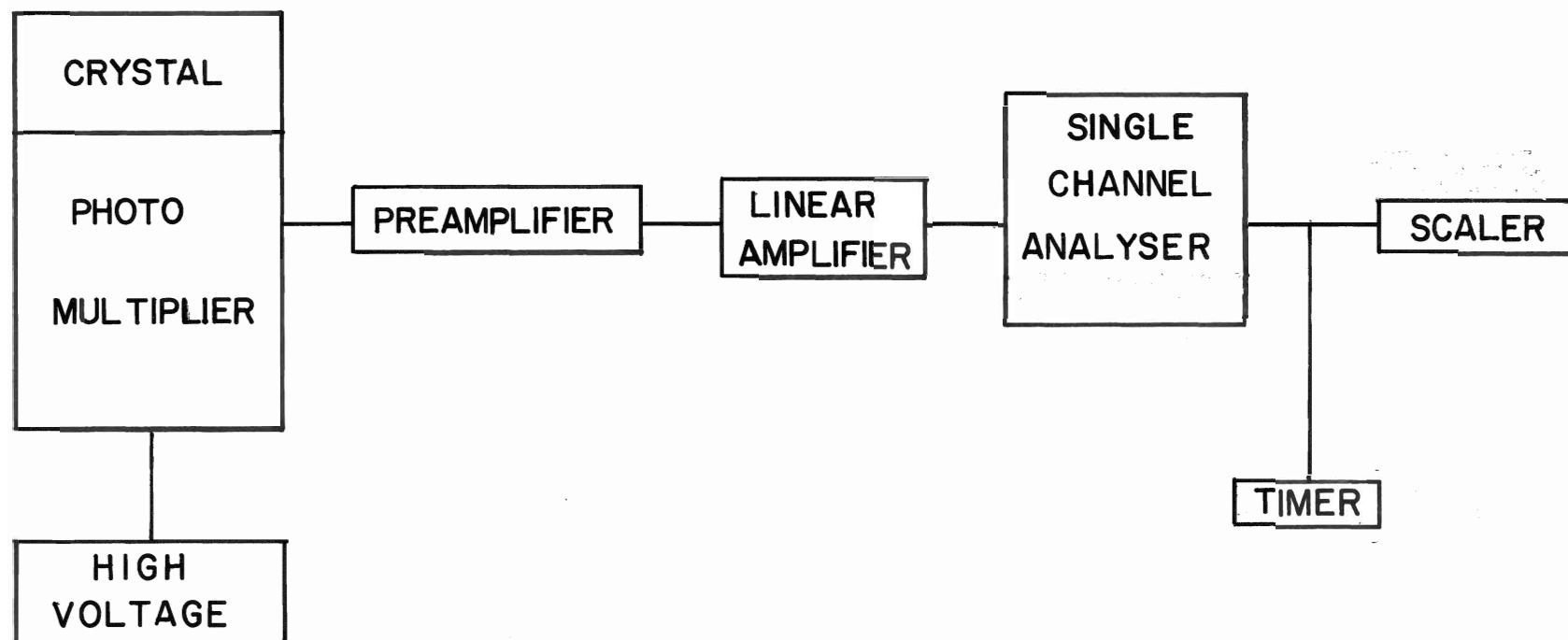


Fig.B.I. Schematic diagram for the measurement of the tracer concentration

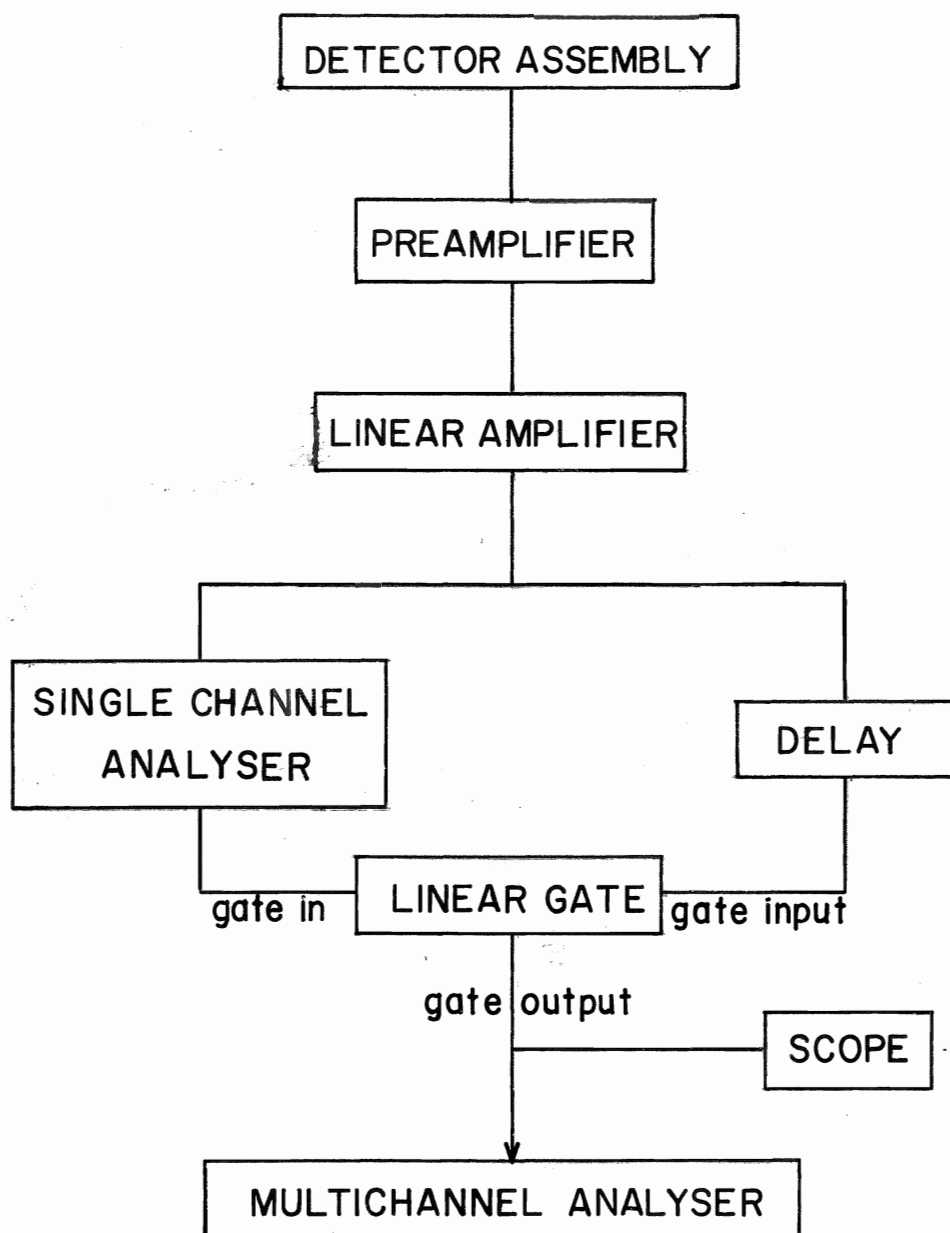


Fig.B.2.Schematic diagram for the calibration of the single channel analyser.

The single channel analyser consists of lower and upper level discriminators. The former is sometimes referred to as "baseline", while the region between the two discriminators is referred to as "window".

The lower level discriminator is initially set at zero and the window at its maximum width. The spectrum is analysed on a multi-channel analyser and the two discriminator levels adjusted until counts within the two  $\text{Co}^{60}$  photopeaks are only being stored. The single channel analyser determines whether each input pulse amplitude is within the window and generates a logic output pulse for each input pulse that satisfies the criteria.

It is preferable, however, to have this logic pulse arrive at the "gate in" position of the linear gate just prior to the arrival of the linear pulse that is to be gated. It is thus necessary to delay the linear pulse by more than one microsecond, as this is approximately the time required for analysing at the single channel analyser.

When the criteria set by the discriminator levels is satisfied, the logic pulse opens the gate for the linear pulse to go through, to the scaler or the multichannel analyser.

The linear gate has a dial on the front panel that controls the gate width from 0.5 to 5 microseconds. In normal operation, when all the modules are properly adjusted, only one pulse will be furnished for the scaler or multichannel analyser.

Figure B.3 shows the two photopeaks, gated from the rest of the spectrum.



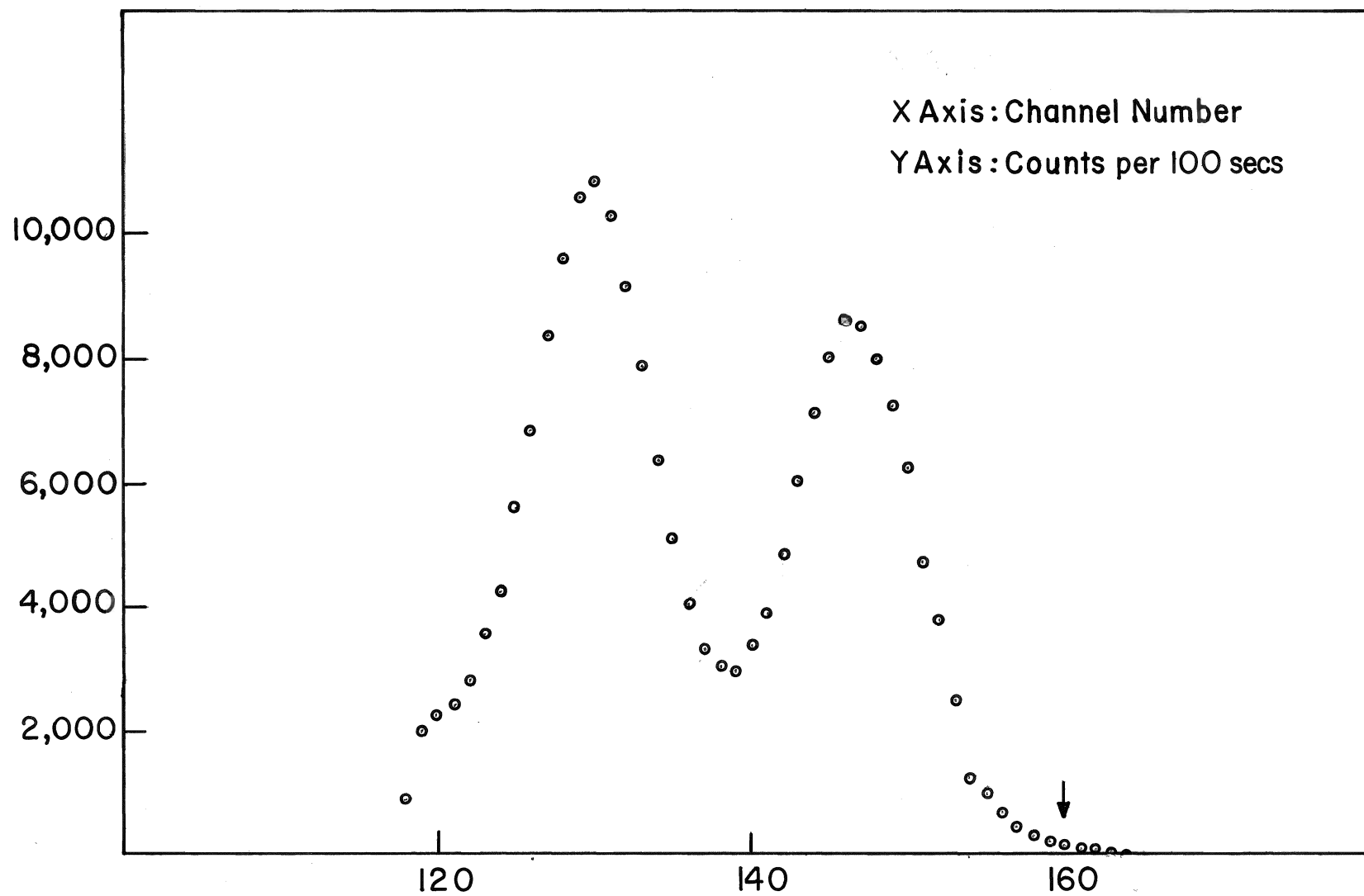


Fig.B.3. Gated  $\text{Co}^{60}$  Spectrum.

### APPENDIX C. General Treatment of Random Walk Processes.

The earlier treatments of the "random walk problem" do not account for a case involving more than one jump mechanism. Even if only a single mechanism is operative, the case involving a large number of segments (or broken series of atomic jumps) had not been considered in detail. It is therefore desirable to have a generalised treatment of the random walk process.

Such a treatment is given in this appendix. It is assumed in the following that a particular atom, say  $k^{\text{th}}$  atom, makes jumps via a number of different mechanisms. The total displacement of the  $k^{\text{th}}$  atom has several segments.

Let  $\vec{R}_{km}$  be the net displacement of the atom after its diffusion through one small segment. As a result of the diffusion, the atom diffuses through jumps in a large number of small segments, and the net total displacement of the  $k^{\text{th}}$  atom,  $\vec{R}_k$ , is given by

$$\vec{R}_k = \sum_m \vec{R}_{km}$$

where  $\vec{R}_{km}$  is the resultant displacement of the  $k^{\text{th}}$  atom in the  $m^{\text{th}}$  segment, and is given by

$$\vec{R}_{km} = \sum_{i=1}^{n_{km}} \vec{r}_{kmi}$$

Here  $\underline{r}_{kmi}$  represents any individual jump, while the upper limit of the summation,  $n_{km}$  defines the total number of jumps made by the atom under consideration, in the  $m^{\text{th}}$  segment.

The square of the net total displacement  $R_k^2$  is given by

$$R_k^2 = \left( \sum_m R_{km} \right)^2 = \sum_m R_{km}^2 + 2 \sum_n \sum_m (R_{km} \cdot R_{kn})$$

and

$$\langle R_k^2 \rangle = \langle \sum_m R_{km}^2 \rangle + 2 \langle \sum_n \sum_m R_{km} \cdot R_{kn} \rangle$$

Clearly, the second term with the double sum above vanishes as the segments are uncorrelated.

Hence,

$$\langle R_k^2 \rangle = \langle \sum_m R_{km}^2 \rangle = \frac{1}{N} \sum_k \left[ \sum_m R_{km}^2 \right] \quad (5.1)$$

where  $N$  represents the total number of atoms considered.

Now, all the squares of the displacements in segments belonging to the same mechanisms are collected together and relabeled.

For example, the segments associated with the  $k^{\text{th}}$  mechanism, may be relabeled as

$$\{R_{km}\}_k, \quad m = 1, 2, 3, \dots, s_{kk}$$

with  $s_{kk}$  representing the segment with the maximum number of jumps made by  $k^{\text{th}}$  atom via  $k^{\text{th}}$  mechanism. As a result, for the  $k^{\text{th}}$  mechanism,

$$\sum_{m=1}^{s_{kk}} R_{km}^2 = \sum_{m=1}^{s_{kk}} \left( \sum_{i=1}^{n_{km}} r_{kmi}^2 \right) + \sum_{m=1}^{s_{kk}} \left[ 2 \sum_{j=1}^{n_{km}-1} \sum_{i=1}^{n_{km}-j} (r_i \cdot r_{j+i})_{km} \right] \quad (5.2)$$

In equation (5.2), the first term contains  $n_{km}$  terms, and, if the length of the jump vector is assumed to be the same for any particular mechanism, the first term in eqn. (5.2) becomes

$$\sum_{m=1}^{s_{kk}} \left( \sum_{i=1}^{n_{km}} r_{kmi}^2 \right) = \sum_{m=1}^{s_{kk}} n_{km} a_k^2 = n_{kk} a_k^2$$

where  $a_k$  is the length of a jump vector for a jump made via  $k^{\text{th}}$  mechanism, and

$$n_{kk} = \sum_{m=1}^{s_{kk}} n_{km}, \quad \text{is the total number}$$

of jumps made by the  $k^{\text{th}}$  atom via  $k^{\text{th}}$  mechanism. Equation (5.2), thus, reduces to,

$$\sum_{m=1}^{s_{kk}} R_{km}^2 = n_{kk} a_k^2 + \sum_{m=1}^{s_{kk}} \left[ 2 \sum_{j=1}^{n_{km}-1} \sum_{i=1}^{n_{km}-j} (r_i \cdot r_{j+i})_{km} \right] \quad (5.3)$$

Taking the average over a large number of atoms  $N$ ,

$$\begin{aligned} \left\langle \sum_{m=1}^{s_{kk}} R_{km}^2 \right\rangle &= \langle R^2 \rangle_k \\ &= \frac{1}{N} \sum_{k=1}^N (n_{kk} a_k^2) + \frac{2}{N} \sum_{k=1}^N \sum_{m=1}^{s_{kk}} \left[ \sum_{j=1}^{n_{km}-1} \sum_{i=1}^{n_{km}-j} (r_i \cdot r_{j+i})_{km} \right] \\ &= \langle n_k \rangle a_k^2 + \frac{2}{N} \sum_{k=1}^N \sum_{m=1}^{s_{kk}} \left[ \sum_{j=1}^{n_{km}-1} \sum_{i=1}^{n_{km}-j} (r_i \cdot r_{j+i})_{km} \right] \end{aligned}$$

$$= a_k^2 \left[ \langle n_k \rangle + \frac{2}{N} \sum_{k=1}^N \sum_{m=1}^{S_{kk}} \left\{ \sum_{j=1}^{n_{km}-1} (n_{km}-j) \overline{\cos \theta_{kmj}} \right\} \right] \quad (5.4)$$

where, we have defined,  $\overline{\cos \theta_{kmj}}$  such that

$$\sum_{i=1}^{n_{km}-1} \underline{r}_i \cdot \underline{r}_{i+j} = a_k^2 (n_{km}-j) \overline{\cos \theta_{kmj}} \quad (5.5)$$

Here,  $\overline{\cos \theta_{kmj}}$  is the average of the cosine of the angle between the vectors separated by  $j$  jumps in the  $m^{\text{th}}$  segment during the displacement of  $k^{\text{th}}$  atom via  $k^{\text{th}}$  mechanism.

Now, irrespective of the segment or the atom (but all for the  $k^{\text{th}}$  mechanism), the segments can be "ordered" such that

$$n_1 < n_2 < n_3 < \dots < n_m < \dots < n_{S_k}$$

where  $n_m$  is the number of jumps made in the  $m^{\text{th}}$  segment,  $n_{S_k}$  is the maximum number of jumps made in a single segment via  $k^{\text{th}}$  mechanism, and  $S_k$  is the total number of segments.

The sum in the second term of equation (5.4)

$$\text{i.e., } \sum_{k=1}^N \sum_{m=1}^{S_{kk}} \left\{ \sum_{j=1}^{n_{km}-1} (n_{km}-j) \overline{\cos \theta_{kmj}} \right\}$$

with this ordering, becomes

$$\begin{aligned} & \sum_{m=1}^{S_k} \sum_{j=1}^{n_1-1} (n_m-j) \overline{\cos \theta_{jm}} + \sum_{m=2}^{S_k} \sum_{j=n_1}^{n_2-1} (n_m-j) \overline{\cos \theta_{jm}} + \dots \\ & \dots + \sum_{m=S_k}^{S_k} \sum_{j=n_{S_k-1}}^{n_{S_k}-1} (n_m-j) \overline{\cos \theta_{jm}} \end{aligned}$$

This can be obtained by expanding the above sum, rewriting it using the requirement  $n_1 < n_2 < \dots < n_{S_k}$ , and then summing down the column.

Thus, expression (5.4) can now be written as

$$\begin{aligned} \langle R^2 \rangle_K = \langle n_K \rangle a_K^2 + 2a_K^2 \left[ \frac{1}{N} \sum_{m=1}^{S_K} \sum_{j=1}^{n_{m-1}} (n_m - j) \overline{\cos \theta_{jm}} + \frac{1}{N} \sum_{m=2}^{S_K} \sum_{j=n_{m-1}}^{n_m-1} (n_m - j) \overline{\cos \theta_{jm}} \right. \\ \left. + \dots + \frac{1}{N} \sum_{m=S_K}^{S_K} \sum_{j=n_{S_K-1}}^{n_{S_K}-1} (n_m - j) \overline{\cos \theta_{jm}} \right] \quad (5.6) \end{aligned}$$

Consider now the first term in the square bracket of eqn. (5.6) for

which  $1 < j < n_{m-1}$ .

Defining  $\langle \cos \theta_j \rangle$  such that

$$\langle \cos \theta_j \rangle \sum_{m=1}^{S_K} (n_m - j) = \sum_{m=1}^{S_K} (n_m - j) \overline{\cos \theta_{jm}},$$

the first term reduces to

$$\frac{1}{N} \sum_{m=1}^{S_K} \sum_{j=1}^{n_{m-1}} (n_m - j) \overline{\cos \theta_{jm}} = \langle n_K \rangle \sum_{j=1}^{n_{m-1}} \left[ 1 - \frac{\langle S_K \rangle}{\langle n_K \rangle} j \right] \langle \cos \theta_j \rangle \quad (5.7)$$

where

$$\langle S_K \rangle = \frac{S_K}{N} \text{ and}$$

$$\langle n_K \rangle = \frac{1}{N} \sum_{m=1}^{S_K} n_m. \quad \#$$

Now, if  $\bar{n}_K$  is the average number of jumps per segment, then we have the requirement

$$N \langle S_K \rangle \bar{n}_K = N \langle n_K \rangle$$

$$\text{i.e., } \bar{n}_K = \frac{\langle n_K \rangle}{\langle S_K \rangle}$$

---

#. The two definitions for  $\langle n_K \rangle$  viz.,  $\langle n_K \rangle = \frac{1}{N} \sum_{k=1}^N \left[ \sum_{m=1}^{S_{Kk}} n_{km} \right]$  and

$$\langle n_K \rangle = \frac{1}{N} \left[ \sum_{m=1}^{S_K} n_m \right] \quad \text{have the same meaning.}$$

With this, equation (5.7) becomes

$$\frac{1}{N} \sum_{m=1}^{S_K} \sum_{j=1}^{n_m-1} (n_m-j) \overline{\cos \theta_{jm}} = \langle n_K \rangle \sum_{j=1}^{n_1-1} \left[ 1 - \frac{j}{n_K} \right] \langle \cos \theta_j \rangle \quad (5.8)$$

Consider now the second term in the square bracket of equation (5.6),

for which  $n_1 < j < n_2 - 1$ .

Defining  $\langle \cos \theta_j \rangle$  such that

$$\langle \cos \theta_j \rangle \sum_{m=2}^{S_K} (n_m-j) = \sum_{m=2}^{S_K} (n_m-j) \overline{\cos \theta_{jm}},$$

the second term reduces to

$$\frac{1}{N} \sum_{m=2}^{S_K} \sum_{j=n_1}^{n_2-1} (n_m-j) \overline{\cos \theta_{jm}} = \langle n_K \rangle \sum_{j=n_1}^{n_2-1} \left[ \left( 1 - \frac{j}{n_K} \right) + \frac{1}{N \langle n_K \rangle} (j - n_1) \right] \langle \cos \theta_j \rangle \quad (5.9)$$

By the same procedure, defining  $\langle \cos \theta_j \rangle$  ( $n_2 < j < n_3 - 1$ ), such that

$$\langle \cos \theta_j \rangle \sum_{m=3}^{S_K} (n_m-j) = \sum_{m=3}^{S_K} (n_m-j) \overline{\cos \theta_{jm}},$$

the third term becomes

$$\frac{1}{N} \sum_{m=3}^{S_K} \sum_{j=n_2}^{n_3-1} (n_m-j) \overline{\cos \theta_{jm}} = \langle n_K \rangle \sum_{j=n_2}^{n_3-1} \langle \cos \theta_j \rangle \left[ \left( 1 - \frac{j}{n_K} \right) + \frac{1}{N \langle n_K \rangle} (2j - n_1 - n_2) \right] \quad (5.10)$$

Or, for any general term  $m$  within the square bracket in the expression

(5.6),

$$\frac{1}{N} \sum_{m=1}^{S_K} \sum_{j=n_{(m-1)}}^{n_m-1} (n_m-j) \overline{\cos \theta_{jm}} = \langle n_K \rangle \sum_{j=n_{(m-1)}}^{n_m-1} \langle \cos \theta_j \rangle \left[ \left( 1 - \frac{j}{n_K} \right) + \frac{1}{N \langle n_K \rangle} \left\{ (m-1)j - n_1 - n_2 - \dots - n_{m-1} \right\} \right]$$

The expression (5.6) can now be rewritten as

$$\begin{aligned} \langle R_K^2 \rangle &= \langle n_K \rangle a_K^2 \left\{ 1 + 2 \left[ \sum_{j=1}^{n_1-1} \left\{ 1 - \frac{j}{n_K} \right\} \langle \cos \theta_j \rangle \right. \right. \\ &\quad \left. \left. + \sum_{j=n_1}^{n_2-1} \left\{ 1 - \frac{j}{n_K} \right\} \langle \cos \theta_j \rangle + \frac{1}{N \langle n_K \rangle} \sum_{j=n_1}^{n_2-1} (j - n_1) \langle \cos \theta_j \rangle \right. \right. \end{aligned}$$

$$\begin{aligned}
& + \sum_{j=n_2}^{n_3-1} \left\{ 1 - \frac{j}{\bar{n}_K} \right\} \langle \cos \theta_j \rangle + \frac{1}{N \langle n_K \rangle} \sum_{j=n_2}^{n_3-1} (2j - n_1 - n_2) \langle \cos \theta_j \rangle \\
& + \sum_{j=n_{(m-1)}}^{(n_{m-1})} \left\{ 1 - \frac{j}{\bar{n}_K} \right\} \langle \cos \theta_j \rangle + \frac{1}{N \langle n_K \rangle} \sum_{j=n_{(m-1)}}^{(n_{m-1})} \{ (m-1)j - n_1 - n_2 \dots - n_{m-1} \} \langle \cos \theta_j \rangle \\
& + \sum_{j=n_{(s_K-1)}}^{(n_{s_K-1})} \left\{ 1 - \frac{j}{\bar{n}_K} \right\} \langle \cos \theta_j \rangle + \frac{1}{N \langle n_K \rangle} \sum_{j=n_{(s_K-1)}}^{(n_{s_K-1})} \{ (s_K-1)j - n_1 - n_2 \dots - n_{(s_K-1)} \} \langle \cos \theta_j \rangle \Bigg\} \\
& = \langle n_K \rangle a_K^2 \left\{ 1 + 2 \left[ \sum_{j=1}^{\bar{n}_K-1} \left\{ 1 - \frac{j}{\bar{n}_K} \right\} \langle \cos \theta_j \rangle \right. \right. \\
& \quad \left. \left. + \sum_{j=\bar{n}_K}^{n_{s_K}-1} \left\{ 1 - \frac{j}{\bar{n}_K} \right\} \langle \cos \theta_j \rangle \right. \right. \\
& \quad \left. \left. + \frac{1}{N \langle n_K \rangle} \sum_{r=1}^{s_K-1} \sum_{j=n_r}^{n_{s_K}-1} (j - n_r) \langle \cos \theta_j \rangle \right] \right\} \quad (5.11)
\end{aligned}$$

$$= \langle n_K \rangle a_K^2 f_K.$$

where

$$\begin{aligned}
f_K &= 1 + 2 \left[ \sum_{j=1}^{\bar{n}_K-1} \left\{ 1 - \frac{j}{\bar{n}_K} \right\} \langle \cos \theta_j \rangle + \sum_{j=\bar{n}_K}^{n_{s_K}-1} \left\{ 1 - \frac{j}{\bar{n}_K} \right\} \langle \cos \theta_j \rangle \right. \\
& \quad \left. + \frac{1}{N \langle n_K \rangle} \sum_{r=1}^{s_K-1} \sum_{j=n_r}^{n_{s_K}-1} (j - n_r) \langle \cos \theta_j \rangle \right] \quad (5.12)
\end{aligned}$$



clearly corresponds to the "correlation factor" previously defined.

When the atoms diffuse through a number of differing mechanisms, the mean square displacement will be given by

$$\langle R^2 \rangle = \sum_K \langle R^2 \rangle_K$$

If  $t$  is the total time for diffusion and  $t_K$ , the time taken for diffusing via  $K^{\text{th}}$  mechanism, we can define  $t_K/t = \lambda_K$  as the fraction of time the atom jumps via the  $K^{\text{th}}$  mechanism where

$$0 < \lambda_K < 1.$$

The observed diffusion coefficient, is then

$$\begin{aligned} D &= \frac{\langle R^2 \rangle}{6t} = \sum_K \frac{\langle R^2 \rangle_K}{6} \frac{\lambda_K}{t_K} \\ &= \sum_K \left( \frac{\langle n_K \rangle}{t_K} \right) \frac{a_K^2 f_K \lambda_K}{6} \\ &= \sum_K \left( \frac{\Gamma_K a_K^2 f_K}{6} \right) \lambda_K \\ &= \sum_K D_K \lambda_K \end{aligned} \tag{5.13}$$

where  $\Gamma_K = \langle n_K \rangle / t_K$  defines the jump frequency for diffusion via  $K^{\text{th}}$  mechanism.

Equation (5.13) gives the general form for the diffusion coefficient, for the case where a number of mechanisms are operative.

#### APPENDIX D. CONCERNING THE "TAIL" IN THE PENETRATION PROFILES

The appearance of the deeply penetrating tail in the penetration profile on the preannealed specimen (figure 4.9) still remains to be accounted for. A number of authors (31,32,33) have attributed profiles similar in appearance to rapid diffusion along dislocation "pipes".

It is, therefore, of interest to analyse the present data in terms of a mathematical model proposed by Suzuoka (34) since the experimental boundary conditions appear to conform closely to those assumed in his study. Suzuoka's model assumes the transportation of atoms through parallel dislocation pipes.

According to this model, the slope  $\gamma$  of the logarithm of the tracer concentration (in the tail) versus the  $6/5^{\text{th}}$  power of the penetration distance is expressed by the relation:

$$0.973 \log_{10}(\Delta - 1) = 6.567 - 1.644 \log_{10} \gamma - \log \sqrt{D_L t} \quad (\text{D.1})$$

where  $\Delta = D_d/D_L$ , is the ratio of the diffusivity along the dislocations to that of the lattice.

The slope  $\gamma$  is obtained from the tail using a least squares fit program as  $\gamma = 1.226$ ; a value of  $8.298 \times 10^{-9} \text{ cm}^2/\text{sec}$  can be obtained for  $D_L$  at  $900^\circ\text{C}$ , from the resolved high temperature curve.

Using Suzuoka's relation (D.1), a value of  $4.860 \text{ cm}^2/\text{sec}$  is obtained for the diffusion coefficient along the dislocation pipes; this is completely unrealistic.

An alternative explanation of the long tail, at least in this study, may be due to the deposition of tracer material on the sides of the specimen with subsequent diffusion into the specimen. In addition to the mass flow from the face (downward flow), an inward flow from the sides could have occurred. The tracer concentration in the various

sections would then be a sum of the downward and the inward mass flow.

The effects due to surface diffusion are, of course, normally eliminated by removing material from the sides before sectioning the specimen on the sides. If, however, an insufficient amount of material was removed, the presence of the deeply penetrating tail might be attributed to this effect.

This surface effect may be pronounced in this particular run as no special care was taken to avoid tracer deposition on the sides of the specimen during the evaporation.

31. J.L. Whitton and G.V. Kidson, Can. J. Phys. 46 2589 (1968).
32. G.P. Williams and L. Slifkin, Phys. Rev. Letters 1 243 (1958).
33. D. Gupta, Phys. Rev. B 7 586 (1973).
34. T. Suzuoka, Trans. Jap. Inst. Metals 2 25 (1961).

## REFERENCES

1. D. Lazarns, Solid State Phys. 10 71 (1960).
2. G. Kidson and J. McGurn, Can. J. Phys. 39 1146 (1961).
3. J.I. Federer and T.S. Lundy, Trans. AIME 227 592 (1963).
4. J.F. Mardock, T.S. Lundy and E.E. Stansbury, Acta Met. 12 1033 (1964).
5. S.J. Rothman, L.T. Lloyd, R. Weil and A.L. Harkness, Trans. AIME 218 605 (1966).
6. G.V. Kidson and R. Ross, Radioisotopes (proc. 1st Unesco Int. Conf., Paris, 1957) p. 185 Pergamon Press, New York (1958).
7. C. Zener, J. Appl. Phys. 22 372 (1951).
8. D. Graham, Diffusion in body centered cubic metals (Cleveland, Ohio: American Society for Metals) p. 27 (1964).
9. C.T. Tomizuka, Acta Met. 6 600 (1958).
10. G.V. Kidson and J.S. Kirkaldy, Phil. Mag. 20 1057 (1969).
11. G.V. Kidson, Diffusion in body centered cubic metals (Cleveland, Ohio: American Society for Metals) p. 329 (1964).
12. G.V. Kidson, Can. J. Phys. 41 1563 (1963).
13. E.W. Hart, Acta Met. 5 597 (1957).
14. G.M. Hood and R.J. Schultz, Phil. Mag. 26 329 (1972).
15. D.L. Gruzin, V.S. Emelyanov, G.G. Ryabova and G.B. Fedorov, A/conf. P/2526 U.S.S.R., p. 187 (1958).
16. G.V. Kidson and G.J. Young, Phil. Mag. 20 1047 (1969).
17. G.V. Kidson, unpublished work.
18. A.D. LeClaire, Phil. Mag. 3 921 (1958).
19. J.R. Manning, Diffusion kinetics for atoms in crystals, D. VanNostrand Company Inc., New Jersey (1968).
20. B.S. Chandrasekhar, Revs. Mod. Phys. 15: 1 (1943).

21. P.G. Shewmon, Diffusion in solids, McGraw-Hill Book Company (1963).
22. K. Compaan and Y. Haven, Trans. Faraday Soc. 52 786 (1956).
23. A.D. LeClaire and A.B. Lidiard, Phil. Mag. Series 8 (I) 518 (1956).
24. A.D. LeClaire, Conf. on Point defects in non-metallic solids, Leamington, Spa. (1963).
25. D.S. Tannhauser, J. Appl. Phys. 27 662 (1956).
26. C.T. Tomizuka, Methods of Expt. Phys. 6 A Solid State Phys., K. Lark Horowitz and V.A. Johnson, Eds. (1959).
27. L.W. Barr, J.N. Mundy and F.A. Smith, Phil. Mag. 14 1299 (1966).
28. A.J. Mortlock, Acta Met. 8 132 (1960).
29. N.F. Fiore and C.L. Bauer, Prog. Mat. Sci. (Progr. Met. Phys., Bruce Chalmers and W. Hume-Rothery, Eds.) 13 85 (1967).
30. D. Graham and E.R. Hanes, NASA TN D-5905 (1970).